J. Fluid Mech. (1999), *vol.* 401, *pp.* 55–84. Printed in the United Kingdom

Experimental study of the stability of deep-water wave trains including wind effects

By TAKUJI WASEDA[1] AND MARSHALL P. TULIN[2]

[1] Frontier Research System for Global Change *and* International Pacific Research Center, University of Hawaii, Honolulu, HI 96822, USA

[2] Ocean Engineering Laboratory, University of California Santa Barbara, CA 93106, USA

(Received 15 December 1998 and in revised form 7 July 1999)

An experimental investigation on the initial instability of nonlinear deep-water wave trains including wind effects is reported. The experiment was conducted at the Ocean Engineering Laboratory wind-wave facility (50 m long, 4.2 m wide, 2.1 m deep), with a fully computer-controlled mechanical wave generator to explore the parameter space: steepness; sideband frequency; wind speed. The estimated growth rates of the Benjamin–Feir instability from seeded wind-free experiments agreed well with the theoretical prediction derived from Krasitskii's four-wave reduced equation as computed here. Wind was added to the same wave system; the growth rates of the sidebands were reduced for weak, and enhanced for strong wind forcing. Experiments with naturally selected sidebands, i.e. unseeded, were conducted as well; measurements showed that wind did not inhibit the growth of sidebands in the case of either two-dimensional or three-dimensional instabilities. A comparison of the results with earlier work suggests that there are two independent effects of wind: first, the alteration of the inviscid growth for a given modulational frequency as shown by comparison with the seeded experiments without wind; second, a change in the natural modulational frequency appearing in the presence of wind which is a function of the wave age, as observed in unseeded experiments. Both effects combined will determine whether the modulational instability is enhanced or suppressed; comparison of experimental results with theoretical predictions suggests that the effect of wind on the natural selection of the modulational frequency is the dominant effect. It was shown that for moderate to old waves, the net effect of wind on the modulational instability is small. For all the experiments except a few unseeded cases with weak breakers, the modulation was small and no breaking was observed within the tank.

1. Introduction

We report here a systematic experimental study of the initial instability of deep-water wave trains (Stokes' waves) including wind effects. Since the report of Benjamin & Feir (1967), a variety of experiments have been conducted to study the evolution of modulational wave trains (Lake *et al.* 1977; Melville 1982; Su *et al.* 1982; Su & Green 1984; Bliven, Huang & Long 1986). Only a few of these were concerned with and measured the initial growth rate of the sidebands or compared measurements with theory. This was partially because the lack of well-controlled wave generators limited the choice of the relevant parameters, $\epsilon \equiv ak$ and $\hat{\delta} \equiv \delta\omega/\epsilon\omega$. The work that we present here is a part of the systematic experimental study conducted in the Ocean Engineering Laboratory large wind-wave facility, partially reported previously

for the long-time evolution of the wave group that includes breaking effects (Tulin & Waseda 1999).

Both Benjamin & Feir (1967) and Lake *et al.* (1977) conducted early experiments for a fixed $\hat{\delta}$ varying ϵ. Those data were compared with a variety of theories (Benjamin 1967; Benjamin & Feir 1967; Lake & Yuen 1977; Yuen & Lake 1982; Janssen 1983). The Benjamin & Feir (1967) theory, which is based on a perturbation approach, was shown by Lake & Yuen (1977) to be reproduced by the nonlinear Schrödinger equation. While Benjamin (1967) showed only fair agreement with theory and experiment, Yuen & Lake (1982) improved theoretical agreement with initial growth rates using Zakharov's theory (Zakharov 1968). Janssen (1983) used the modified nonlinear Schrödinger equation (Dysthe 1979) to predict initial growth rates, and showed a significant improvement over nonlinear Schrödinger equation predictions. Although theories that include finite-amplitude effects (Zakharov 1968; Dysthe 1979), show significant improvement over the linear instability analysis of Benjamin (1967), their validity is still limited to relatively small steepnesses; this may readily be seen in a diagram showing predictions of the fastest growing modulational frequency against steepness (Dysthe 1979; Longuet-Higgins 1980; Yuen & Lake 1982). Zakharov's theory agrees with the exact solution of Longuet-Higgins up to moderate steepness while Dysthe's theory fails for relatively small steepness ($\epsilon < 0.1$).

To extend available data without wind, we have conducted a set of experiments for a fixed ϵ varying $\hat{\delta}$. Seeded experiments were conducted with a wave-generator motion controlled by prescribing ϵ, $\hat{\delta}$, and the initial modulation ('seeded'). The resulting surface elevation time series were obtained from 11 stations along the tank, allowing us to obtain a reliable growth rate estimate. The measured growth rates were in reasonable agreement with those computed by us using the theory of Krasitskii (1994).

For some selected cases, we have added wind. The wind speed was varied (1.8–13.1 m s^{-1}, wave ages $C_p/U_{1m} = 0.12$–0.87, or $C_p/u_* = 1.8$–7.4) and the growth rate estimates were compared with the no wind cases; here C_p is the phase velocity, U_{1m} is the mean wind speed at 1 m height, and u_* is the friction velocity. The comparison showed that the influence of wind depends on wave age; growth is suppressed with moderately old and old waves but enhanced with young waves.

In addition to these experiments, a long run of a monochromatic wave was conducted with and without wind. Sidebands develop naturally due to the disturbance originating from the wave front which propagates between the wave generator and the beach (Melville 1982; Tulin & Waseda 1999). Such 'unseeded' experiments are similar to the experiments conducted by Bliven *et al.* (1986) and Li, Hui & Donelan (1988). In disagreement with these earlier works, the sideband growth was observed to be not necessarily suppressed by the wind. However, the natural sideband frequencies varied with the wind speed. Changes in the growth rate would therefore seem at least partially due to the resulting differences in modulational frequency between the Bliven *et al.* (1986) and the present results.

For the largest wave steepnesses here ($\epsilon = 0.20$ and 0.24), the case $\epsilon = 0.24$ displayed a three-dimensional instability, so-called type II instability (McLean 1982). The sideband frequency was in this case close to that observed by Su (1982). Although the sideband growth was affected at the higher wind speed, the growth rates were not suppressed.

Section 2 briefly describes the theoretical background. In § 3, the experimental procedure and the analysis method are discussed in detail. The results are presented in § 4. A discussion is given in § 5 and the conclusions follow.

2. Instability theory

The water surface elevation of the sideband system can be approximated as

$$\zeta(x,t) = a\,\mathrm{e}^{\mathrm{i}\alpha}\,\mathrm{e}^{\mathrm{i}(k_0x-\omega_0t)} + b_+\,\mathrm{e}^{\mathrm{i}\beta_+}\,\mathrm{e}^{\mathrm{i}(k_+x-\omega_+t)} + b_-\,\mathrm{e}^{\mathrm{i}\beta_-}\,\mathrm{e}^{\mathrm{i}(k_-x-\omega_-t)}, \tag{2.1}$$

where a, b_+, and b_- are the real amplitudes; α, β_+, and β_- are the real phases of the wave modes; k_0, k_+, and k_- are the wavenumbers and ω_0, ω_+, and ω_- are the wave frequencies satisfying

$$\left.\begin{array}{c} 2\omega_0 - \omega_+ - \omega_- = 0, \\ 2k_0 - k_+ - k_- = \Delta k, \\ \omega_\pm = \omega_0(1 \pm \delta). \end{array}\right\} \tag{2.2}$$

Here, the sideband amplitudes b_+ and b_- are much smaller than the carrier wave amplitude a. The steepness ϵ is defined as $(ak)_0$. The wave system described by (2.1) is a simplified representation of a three-component wave train with moderate steepness undergoing two-dimensional modulation. The detuning parameter is $\Delta k = -2\delta^2 k_0$ for waves satisfying the linear dispersion relation $\omega^2 = gk$.

Because of nonlinear interaction among wave modes, the sideband waves will grow exponentially. The initial growth rate, $\beta_x = \mathrm{d}(\ln b_\pm)/\mathrm{d}(kx)$, is predicted by the perturbation analysis of Benjamin & Feir (1967):

$$\beta_{BF} = \epsilon^2\,\hat{\delta}\,(2.0 - \hat{\delta}^2)^{1/2}, \tag{2.3}$$

where $\hat{\delta} = \delta/\epsilon$, with the condition for the instability, $0 < \hat{\delta} \leqslant \sqrt{2}$. Thus, the normalized growth rate β_{BF}/ϵ^2 does not explicitly depend on ϵ.

Phillips (1967) derived the Benjamin–Feir instability within the framework of the nonlinear wave–wave interaction theory. He has shown, to the first order in amplitudes, that the combination of resonant de-tuning and amplitude dispersion is the essential ingredient in the Benjamin–Feir instability of the Stokes' wave, and has derived the exponential growth rate starting from the Benney (1962) interaction equation. A similar approach has been taken by Yuen & Lake (1982), deriving the initial growth rate of the sideband instability starting from the Zakharov interaction equation. Such studies showed that the normalized growth rate β_x/ϵ^2 depends on both ϵ and $\hat{\delta}$, and the instability range depends on ϵ.

We have derived the evolution equation for the sideband system by using Krasitskii's (1994) reduced four-wave equation (see the Appendix for the derivation). To the leading order and neglecting higher-order terms such as b_+^2, b_-^2, and b_+b_-, we obtain

$$\left.\begin{array}{l} \dfrac{\mathrm{d}a}{\mathrm{d}\tilde{x}} = 0, \quad \dfrac{\mathrm{d}b_+}{\mathrm{d}\tilde{x}} = C_+\,\epsilon^2 b_-\,\sin\phi, \quad \dfrac{\mathrm{d}b_-}{\mathrm{d}\tilde{x}} = C_-\,\epsilon^2 b_+\,\sin\phi, \\ \dfrac{\mathrm{d}\phi}{\mathrm{d}\tilde{x}} = 2\left(\dfrac{\omega_0}{2k_0}\left(\dfrac{\omega_+}{2k_+}\right)^{-1} T_{1212} + \dfrac{\omega_0}{2k_0}\left(\dfrac{\omega_-}{2k_-}\right)^{-1} T_{1313} - T_{1111}\right)\epsilon^2 \\ \qquad\qquad +2(C_+C_-)^{1/2}\,\epsilon^2\,\cos\phi - \Delta k/k, \end{array}\right\} \tag{2.4}$$

where $\tilde{x} \equiv kx$, $\phi \equiv 2\alpha - \beta_+ - \beta_- - \Delta k x$, $C_+ \equiv (\omega_0/2k_0)(\omega_-/2k_-)^{1/2}(\omega_+/2k_+)^{-3/2}T_{1123}$ and $C_- \equiv (\omega_0/2k_0)(\omega_+/2k_+)^{1/2}(\omega_-/2k_-)^{-3/2}T_{1123}$; the T are the interaction coefficients

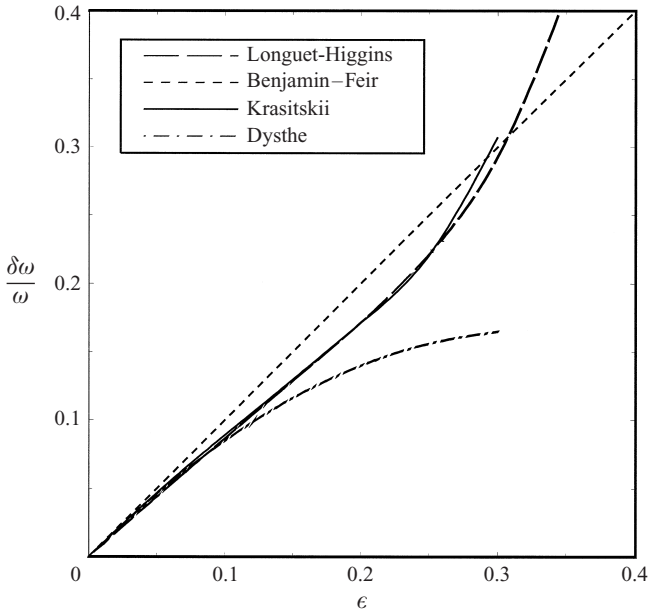

FIGURE 1. The most unstable modulational frequency as a function of ϵ. Theories from Longuet-Higgins (1980), Benjamin & Feir (1968) and Dysthe (1979) are compared with (2.5) derived from Krasitskii (1994).

derived by Krasitskii (1994), where subscripts 1, 2 and 3 stand for the carrier, the lower and the upper sidebands respectively. Solutions of (2.4) yield a set of equations to determine the initial growth rate and related quantities:

$$\left.\begin{aligned} b_+ &= (C_+/C_-)^{1/2}\, b_- = b_+(0)\exp\left[\beta_K \tilde{x}\right] = (C_+/C_-)^{1/2} b_-(0)\exp\left[\beta_K \tilde{x}\right], \\ \cos\phi &= 0.5\left[\frac{\Delta k/k}{\epsilon^2} - \left(\frac{\omega_0}{2k_0}\left(\frac{\omega_+}{k_+}\right)^{-1} T_{1212} + \frac{\omega_0}{2k_0}\left(\frac{\omega_-}{k_-}\right)^{-1} T_{1313} - 2\,T_{1111}\right)\right] \\ &\quad \times (C_+C_-)^{-1/2}, \\ \beta_K &= \epsilon^2 (C_+C_-)^{1/2}\,\sin\phi, \end{aligned}\right\} \tag{2.5}$$

which may easily be computed. In figure 1, we compare the prediction of the most unstable modulational frequency as a function of ϵ with various different theories (Benjamin & Feir 1967; Dysthe 1979; Longuet-Higgins 1980; Krasitskii 1994). From this, we see that the computation using (2.5) agrees very well with the exact theory of Longuet-Higgins (1980) and provides strong support for the validity of the present Krasitskii type calculation.

Equation (2.4) can be rewritten using normalized variables, $\tilde{b}_+ \equiv b_+/a$ and $\tilde{b}_- \equiv b_-/a$:

$$\left.\begin{aligned} \frac{\mathrm{d}\tilde{b}_+}{\mathrm{d}\tilde{x}} &= C_+\epsilon^2 \tilde{b}_-\,\sin\phi = C\,\beta_K\,\tilde{b}_-, \\ \frac{\mathrm{d}\tilde{b}_-}{\mathrm{d}\tilde{x}} &= C_-\epsilon^2 \tilde{b}_+\,\sin\phi = \frac{1}{C}\,\beta_K\,\tilde{b}_+, \end{aligned}\right\} \tag{2.6}$$

where $C \equiv (C_+/C_-)^{1/2}$ and β_K are given by (2.5). Now we further define a new variable, the mean normalized sideband amplitude:

$$\bar{b} \equiv 0.5(\tilde{b}_+ + C\,\tilde{b}_-). \tag{2.7}$$

Using this new variable, the evolution equations (2.6) may be combined to give

$$\frac{\mathrm{d}\bar{b}}{\mathrm{d}\tilde{x}} = \beta_K\,\bar{b}. \tag{2.8}$$

We finally define the growth rate of the sideband as

$$\beta_x \equiv \frac{\mathrm{d}\bar{b}/\mathrm{d}\tilde{x}}{\bar{b}}, \tag{2.9}$$

which can be used directly when estimating the growth rate from experimental data.

The effect of wind may in principle be added to the instability analysis, since a linear wind-wave growth has been deduced in the field by Snyder *et al.* (1981):

$$\beta_s = C_s\left(\frac{U}{C_p} - 1.0\right), \tag{2.10}$$

where U is the mean wind speed, C_p is the wave celerity, and $C_s = 0.000942$ is an empirical constant.

Adding (2.10) to (2.4) and rewriting (2.4) using normalized variables, $\tilde{b}_+ \equiv b_+/a$ and $\tilde{b}_- \equiv b_-/a$, as in (2.6), we obtain

$$\left.\begin{aligned}\frac{\mathrm{d}\tilde{b}_+}{\mathrm{d}\tilde{x}} &= C\,\beta_K\,\tilde{b}_- + C_s\delta\left(\frac{U}{C_p}\right)\tilde{b}_+,\\ \frac{\mathrm{d}\tilde{b}_-}{\mathrm{d}\tilde{x}} &= \frac{1}{C}\,\beta_K\,\tilde{b}_+ - C_s\delta\left(\frac{U}{C_p}\right)\tilde{b}_-.\end{aligned}\right\} \tag{2.11}$$

For $\epsilon \sim \delta \sim 10^{-1}$, the first term is $O(10^{-2})$ and the second term is $O(10^{-4})$ for $U/C_p \sim O(1)$; therefore, the second term is small, indicating the weak effect of wind on the growth of normalized variables. Oshri (1996) obtained a more rigorous derivation of the effect of the wind input on the instability by extending the wave interaction theory of Krasitskii (1994) and also showed that the effect of wind on the normalized sideband is nearly negligible; in his analysis, the effect of wind was introduced to the wave system through application of a suitable normal pressure distribution along the wave. He has shown that the effect of wind will not change the higher-order terms that are responsible for the instability. This justifies the linear superposition of the wind input term in (2.11), as far as the initial instability is concerned. As the waves grow as a result of wind–wave interactions, the terms neglected in the initial instability analysis become significant. Also, strong wind–wave interactions as observed in various experimental studies may become important as well (Phillips & Banner 1974; Toba *et al.* 1986). The linear superposition of the wind input term is no longer valid, but such cases are beyond the scope of our study since our main concern is the initial instability.

Using the new mean sideband variable, (2.7), the evolution equations (2.11) may be combined as before:

$$\frac{\mathrm{d}\bar{b}}{\mathrm{d}\tilde{x}} = \beta_x\,\bar{b} + 0.5\frac{U}{C_p}\delta C_s(\tilde{b}_+ - C\,\tilde{b}_-). \tag{2.12}$$

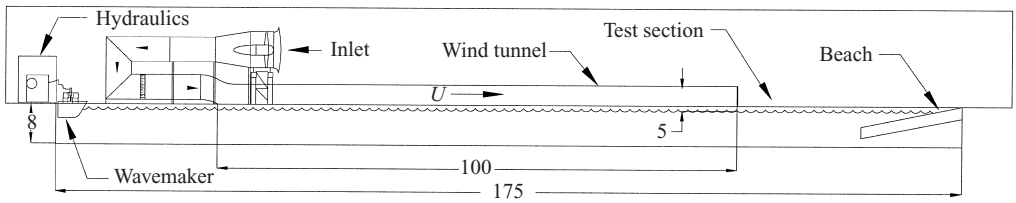

FIGURE 2. Ocean Engineering Laboratory (UCSB) wind-wave tank. Wavemaker: computer-driven bi-modal plunger; $\lambda \sim 0.6-10$ m. Wind tunnel: maximum flow rate of 13 m s^{-1}. Dimensions are in feet.

Again the second term of (2.12) is nearly negligible, since $\tilde{b}_+ - C\,\tilde{b}_- = O(\delta)$, and therefore (2.9) should provide a good estimate from experiments of the sideband growth rate due to nonlinear interactions, excluding the effect of the wave growth by wind.

3. Experiments and analyses

3.1. *Facility and instrumentation*

The experiment was conducted at the large wind-wave facility at the University of California, Santa Barbara (Tulin & Waseda 1999); see figure 2. The tank is 50 m long, 4.2 m wide, 2.1 m deep; the open circuit tunnel section starts at around 8 m fetch and ends at 38 m fetch, and the air passage height is 1.5 m. The waves were generated by a hydraulically actuated plunger, controlled by a computer-generated signal. The maximum wind speed is 13 m s^{-1} at the end of the wind tunnel section. The wave reflection from the beach is typically less than 3% in amplitude; less than 1% in energy.

Waves that can be generated range from about 60 cm to 4 m wavelength. Typically, for the study of unstable wave trains, we have used waves over 1.5 m or so. Those waves tend to be planar due to the wave guide effect as discussed in Tulin & Waseda (1999). We can generate seeded unstable wave trains in the range of 1–4 m wavelength and steepness 0.12–0.28.

Surface elevation time series were obtained using an array of wave wires placed along the tank (a total of 11 wires placed at fetches 1.2, 12.64, 15.64, 18.64, 21.64, 24.64, 27.64, 30.64, 33.64, 36.64 and 41.14 m). The capacitance-type wave wires (0.4 mm diameter anodized tantalum wire), the sensing circuitry, and the digitizing circuitry were made at the OEL. Each wire had a dynamic range of $\sim$ 60 cm at 12 bits digitization, with noise typically less than 4 counts ($\sim$ 0.5 mm). The linearity of the wires was ensured by static calibration.

The wind speeds were monitored at the end of the tunnel section, at 1 m above mean water level (U_{1m}). The anemometer was vertically traversed above the mean water level in order to obtain the mean wind velocity profile. The velocity profile was used to estimate the friction velocity u_*. These measured wind-related parameters are used to define wave ages: C_p/U_{1m} and C_p/u_*. Their inverse values are presented in table 1. The more commonly used wave age defined as C_p/U_{10m} can easily be obtained by extending the logarithmic profile, and in the current experiment, the correction gave $C_p/U_{10m} \sim 1.3 \times C_p/U_{1m}$.

The data acquisition was PC based, and the software was developed by National

	λ (m)	f_c (Hz)	ϵ	δf (Hz)	f_+ (Hz)	f_- (Hz)	b_+/a	$\hat{\delta}$
Sideband system without wind								
SB1NW01	1.56	1.0	0.175	0.06	1.06	0.94	0.01	0.343
SB1NW02	1.56	1.0	0.175	0.09	1.09	0.91	0.01	0.514
SB1NW03	1.56	1.0	0.175	0.12	1.12	0.88	0.01	0.686
SB1NW04	1.56	1.0	0.175	0.15	1.15	0.85	0.01	0.857
SB1NW05	1.56	1.0	0.175	0.18	1.18	0.82	0.01	1.029
SB2NW01	1.56	1.0	0.133	0.112	1.112	0.888	0.01	0.842

	λ (m)	f_c (Hz)	ϵ	b_+/a	$\hat{\delta}$	U_{1m} (m s^{-1})	u_* (cm s^{-1})	U_{1m}/C_p	u_*/C_p	Ω
Sideband system with wind										
SB1W01	1.56	1.0	0.175	0.01	0.857	1.8	—	1.15	—	26.6
SB1W02	1.56	1.0	0.175	0.01	0.857	4.1	29.3	2.63	0.188	11.6
SB1W03	1.56	1.0	0.175	0.01	0.857	6.3	37.1	4.04	0.238	7.6
SB1W04	1.56	1.0	0.175	0.01	0.857	8.5	41.3	5.45	0.265	5.6
SB1W05	1.56	1.0	0.175	0.01	0.857	10.8	47.6	6.92	0.305	4.4
SB1W06	1.56	1.0	0.175	0.01	0.857	13.1	64.4	8.4	0.413	3.6
SB2W01	1.56	1.0	0.133	0.01	0.842	1.8	—	1.15	—	15.4
SB2W02	1.56	1.0	0.133	0.01	0.842	4.1	21.9	2.63	0.135	6.7
SB2W03	1.56	1.0	0.133	0.01	0.842	6.3	35.6	4.04	0.228	4.4
SB2W04	1.56	1.0	0.133	0.01	0.842	8.5	39.2	5.45	0.251	3.2
SB2W05	1.56	1.0	0.133	0.01	0.842	10.8	50.3	6.92	0.322	2.6
SB2W06	1.56	1.0	0.133	0.01	0.842	13.1	60.8	8.4	0.390	2.1
Monochromatic wave with and without wind										
M1W01	1.56	1.0	0.24	—	(1.104)	0	0	0	0	—
M1W02	1.56	1.0	0.24	—	(1.104)	4.1	—	2.63	—	—
M1W03	1.56	1.0	0.24	—	(1.188)	8.5	—	5.45	—	—
M1W04	1.56	1.0	0.24	—	—	13.1	—	8.4	—	—
M2W01	1.56	1.0	0.20	—	(0.679)	0	0	0	0	—
M2W02	1.56	1.0	0.20	—	(0.679)	1.8	—	1.15	—	34.8
M2W03	1.56	1.0	0.20	—	(0.763)	4.1	30.9	2.63	0.198	15.2
M2W04	1.56	1.0	0.20	—	(0.810)	6.3	35.2	4.04	0.226	9.9
M2W05	1.56	1.0	0.20	—	(0.894)	8.5	37.8	5.45	0.242	7.3
M2W06	1.56	1.0	0.20	—	(0.965)	10.8	50.6	6.92	0.324	5.8
M2W07	1.56	1.0	0.20	—	—	13.1	85.4	8.4	0.547	4.8

TABLE 1. Experimental conditions summary.

Instrument LabVIEW. The water surface-elevation time series were acquired at a 41 Hz data rate and stored.

3.2. *Wave-generator signal*

The generation of the unstable Stokes' wave train was discussed in detail in Tulin & Waseda (1999), and therefore we will only report a short summary here. The wave

form signal used to control the wave generator is

$$Y(t) = e(t)\frac{s}{2}\left[\frac{a}{a_0}\cos(\omega_0 t) + \frac{b_+}{a_0}\cos(\omega_+ t + \phi_+) + \frac{b_-}{a_0}\cos(\omega_- t + \phi_-)\right], \tag{3.1}$$

where the ramp used to start and terminate the wave-generator motion is

$$e(t) = \begin{cases} \frac{1}{2}\left(1 - \cos(\pi t/\tau)\right), & 0 \leqslant t \leqslant \tau \\ 1, & \tau < t < T - \tau \\ \frac{1}{2}\left(1 - \cos(\pi\,(t - T)/\tau)\right), & T - \tau \leqslant t \leqslant T, \end{cases} \tag{3.2}$$

where $T = 240$ s is the total length of the data, and s is the stroke in arbitrary units. Here a, b_+, and b_- satisfy

$$a_0^2 = a^2 + b_+^2 + b_-^2, \tag{3.3}$$

where a_0 is the amplitude of the unmodulated wave train. In all runs, the initial phases ϕ_+ and ϕ_- were set to $-\pi/4$, satisfying the maximum growth condition ($\phi_+ + \phi_- = -\pi/2$) predicted by Benjamin & Feir (1967). Furthermore, b_+ and b_- were set equal. Then, for a given wavelength, the choice of parameters is

$$\epsilon, \quad b_\pm/a_0, \quad \text{and} \quad \hat{\delta}. \tag{3.4}$$

The disturbances in the tank cause amplification of selective wave modes in a resonant wave interaction experiment (Hammack & Henderson 1993). The sources of disturbance and their effect on the evolution of the modulational wave train was reported in detail in Tulin & Waseda (1999). They showed that the selection of the naturally grown sidebands comes from the multiple reflection of the wave train front within the tank. In the current experiment, we have limited the duration of the run in order to minimize influences of such disturbances for the seeded case. For the unseeded case, the measurement was initiated after these naturally grown sidebands have been selected.

Once the parameters were set, the time series of the wave-generator signal was computed and stored as digital data, which were transmitted to the wave-generator controller at 200 Hz. The communication between the computer and the controller was fully digital, which makes the transfer noise immune.

3.3. *Experimental procedure*

The experimental procedure for the seeded test with wind was as follows: first the wind was started over still water; once the wind waves in the tank were fully developed, the wave generator was initiated; the data were acquired, and then both the fan and the wave generator were stopped. For the case without wind, the wave generator was initiated with still water.

The run was repeated five times. After each run, both the wind and the wave generator were stopped and the tank was left undisturbed until the residual waves from the previous run had disappeared; the surface-elevation spectrum was observed in real time.

The case of monochromatic wave with wind, the unseeded test, was conducted differently. First, the wave generator was started to generate a monochromatic wave train. Then, after about two to three minutes, the wind was initiated. Whether with or without wind, it took about 10 minutes until the waves started to naturally modulate. Therefore, of the total data length of about 60 min, the first 10 min were not used for the computation of the spectrum.

3.4. *Analysis techniques*

The growth rate β_x was estimated from the surface elevation time series in the following steps: (i) a spectral estimate was obtained from the time series; (ii) the amplitude of each mode was estimated from the spectrum; (iii) the normalized sideband amplitudes were plotted against fetch, and the model equation was fitted to estimate the growth rate.

The spectral estimate was obtained from the surface-elevation time series using a discrete Fourier transformation with the Hanning window applied. The frequency resolution of the spectrum was around 0.01 Hz, small enough to distinguish different wave modes; the separation between the carrier wave and the sideband waves δf ranged from 0.06 to 0.18 Hz. From the spectrum the amplitudes of the wave modes were estimated: the amplitudes of each wave mode were estimated as the square root of the total energy of the spectral peaks, integrating the contributions from the neighbouring frequency bins; by doing so, we may compensate for the leakage of the spectral energy due to the effect of finite data length. The resulting sideband amplitudes were then normalized by the carrier wave amplitude. The mean normalized amplitudes $\overline{b}$ were computed using (2.7), and those were averaged over five independent yet identical-condition runs in order to obtain the mean normalized amplitude estimates and the standard deviation. Then, the average mean normalized sideband amplitudes were plotted versus non-dimensional fetch, and the growth rate was estimated fitting a model equation to the data:

$$\overline{b}(\tilde{x}) = \overline{b}(0)\,\exp(\beta_x\,\tilde{x}), \tag{3.5}$$

using the Levenberg–Marquardt method, where $\overline{b}(0)$ and β_x are the parameters to be estimated.

The analysis method described here is slightly different from the technique first suggested by Lake *et al.* (1977), which was later adopted by Melville (1982). They treated the upper and the lower sidebands independently, and the actual growth rate was computed by fitting the model equation to one of them. Both Lake *et al.*'s (1977) and Melville's (1982) data included a strongly modulated stage, and therefore the resulting growth is no longer in the initial stage. Thus, for this study, we have chosen a small initial sideband amplitude ($b_{\pm}/a = 0.01$); the modulation at the end of the tank was still small ($b_{\pm}/a \sim 0.1$). This allows us to better estimate the initial growth rate of the sideband wave modes.

The use of the normalized sideband amplitude removes the first-order effect of dissipation (Lake *et al.* 1977). Furthermore, the normalization of the sideband helps allow removal of the experimental uncertainties caused by uncalibrated wave wires, and the cross-tank bias.

As a final remark, we should mention that the qualitative picture as a whole will not change even if the growth rates are estimated using different analysis schemes. Therefore, the conclusions of this paper would not change even if we used the method suggested by Lake *et al.* (1977).

4. Results

4.1. *Experimental conditions*

Experiments were conducted for the following wave systems: (i) sideband system without wind (SB1NW, SB2NW); (ii) sideband system with wind (SB1W, SB2W); (iii)

monochromatic wave with and without wind (M1W, M2W). Experiments (i) and (ii) are the seeded experiments and (iii) is the unseeded experiment.

For all the experiments, the carrier wave frequencies were fixed at 1.0 Hz (1.56 m) and for the seeded cases the initial sideband amplitudes were fixed at $b_{\pm}/a = 0.01$. The parameters ϵ, $\hat{\delta}$, and U_{1m} varied and are summarized in table 1. For the seeded sideband systems without wind, we chose two moderate steepnesses close to that of a typical ocean wave, $\epsilon = 0.175$ and 0.133; for $\epsilon = 0.175$ (SB1NW), we varied the normalized modulational frequency $\hat{\delta}$ from 0.343 to 1.029 in five steps, well within the instability condition, and for $\epsilon = 0.133$ (SB2NW), we fixed the normalized modulational frequency $\hat{\delta}$ at 0.842. The case SB1NW04 ($\hat{\delta} = 0.857$) roughly corresponds to the maximum growth condition for $\epsilon = 0.175$, and the case SB2NW01 ($\hat{\delta} = 0.842$) roughly corresponds to the maximum growth condition for $\epsilon = 0.133$, as expected from the theory. These two cases, SB1NW04 and SB2NW01, were used to study the influence of wind. For each case, the wind speeds were varied in six steps between 1.8 m s^{-1} and 13.1 m s^{-1}. The wave ages, C_p/U_{1m}, ranged from $O(0.1)$ to $O(1.0)$, corresponding to moderately old to old sea.

The unseeded experiments were carried out for steepnesses $\epsilon = 0.24$ (M1W) and 0.20 (M2W); the wind was added at six speeds between 1.8 m s^{-1} and 13.1 m s^{-1}. A steepness slightly larger than the seeded case was used in order to observe sufficiently large sideband evolution in the tank. For steepness $\epsilon = 0.175$, the naturally selected sidebands were not observed. The initial amplitudes of the naturally emerging sidebands and their modulational frequencies varied among experiments and the latter are summarized in table 1, indicated by parentheses. The $\epsilon = 0.2$ cases (M2W) displayed a type I (two-dimensional) instability whereas the larger steepness cases, $\epsilon = 0.24$, (M1W) displayed type II (three-dimensional). This natural selection of the sideband in the tank will be further discussed later.

4.2. *Seeded cases, with and without wind*

4.2.1. *Spectrum*

We first describe the spectrum of the seeded cases. Spectra at fetch 41.14 m are shown for wind speeds 4.1, 8.5, and 13.1 m s^{-1} for $\epsilon = 0.175$, $\hat{\delta} = 0.857$, figure 3, and for $\epsilon = 0.133$, $\hat{\delta} = 0.842$, figure 4. The wind-free seeded case (middle curves) as well as the wind-alone case (bottom curves) are plotted together as a reference. The spectral evolution without wind was described in detail in Tulin & Waseda (1999) for a long time evolution, and some of the features described there are found in the spectrum shown here for a much earlier stage. For example, the discrete energy peaks at high frequencies that are bound to the three main waves around 1 Hz, are found here for the 0 m s^{-1} cases (SB1NW04, SB2NW01). These spectral peaks are very narrow and the energy is usually confined to a single frequency bin. The peaks grow in magnitude as the modulation increases and play an important role in the longer time evolution of the three main waves as described in Tulin & Waseda. Particularly, the asymmetry of the upper and the lower sideband evolution is due to the generation of these high-frequency peaks. At the early stage evolution studied here, the asymmetry of the upper and the lower sidebands is not yet obvious.

For the cases with wind, the gaps between these spectral peaks tend to be filled in as the wind speed increases. However, some of the main spectral peaks such as the second and the third harmonics of the carrier wave and their sidebands are still visible. In fact, their energy levels have not reduced, rather they have increased with wind speed. The wind-wave spectrum was obtained without mechanically generated

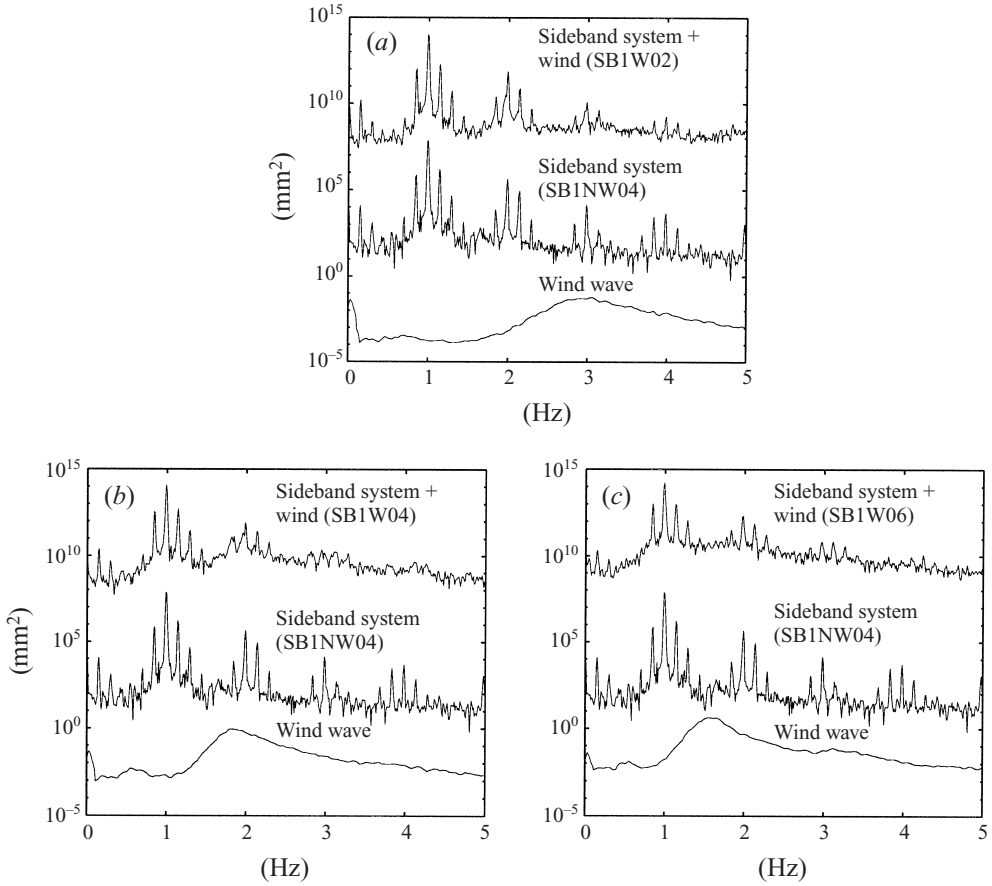

FIGURE 3. Spectrum of the seeded sideband wave system (1.0 Hz, $\epsilon = 0.175$) with wind (SB1W02, SB1W04 and SB1W06), plotted together with the no-wind case (SB1NW04) and the wind-wave spectrum. The spectral estimates are approximately 10 degrees of freedom, frequency resolution 0.01 Hz, and Hanning window was applied. The spectra have an offset of five decades. Wind speeds are (*a*) 4.1, (*b*) 8.5, (*c*) 13.1 m s^{-1}. Fetch is 41.14 m.

background waves. These wind-wave spectral peaks are not visible in figures 3 and 4 (top curves), indicating that they were suppressed in the presence of mechanically generated sideband waves. The suppressed wind-wave energy is much larger than the wind-wave energy that filled the gaps between the high-frequency peaks. In general the suppressed wind-wave energy due to background waves ranges between 60% and 80%. It is important to point out here that, for all the wind speeds we tested, the wind-wave spectral peaks are much larger than 1.0 Hz. Therefore, for all the runs we made, these peaks never reached the mechanically generated wave frequency. Therefore, the main three waves, 0.85 Hz, 1.00 Hz and 1.15 Hz for $\epsilon = 0.175$, and 0.888 Hz, 1.00 Hz and 1.112 Hz for $\epsilon = 0.133$, are far from merging into the wind-wave spectrum; thus the peaks are narrow and frequencies fixed even when the wind is present.

4.2.2. *Growth versus fetch*

The sideband energy was computed from the spectrum, and the variable $\bar{b}$ (2.7) thus obtained is plotted in the fetch evolution diagrams (figures 5, 6 and 7). The error

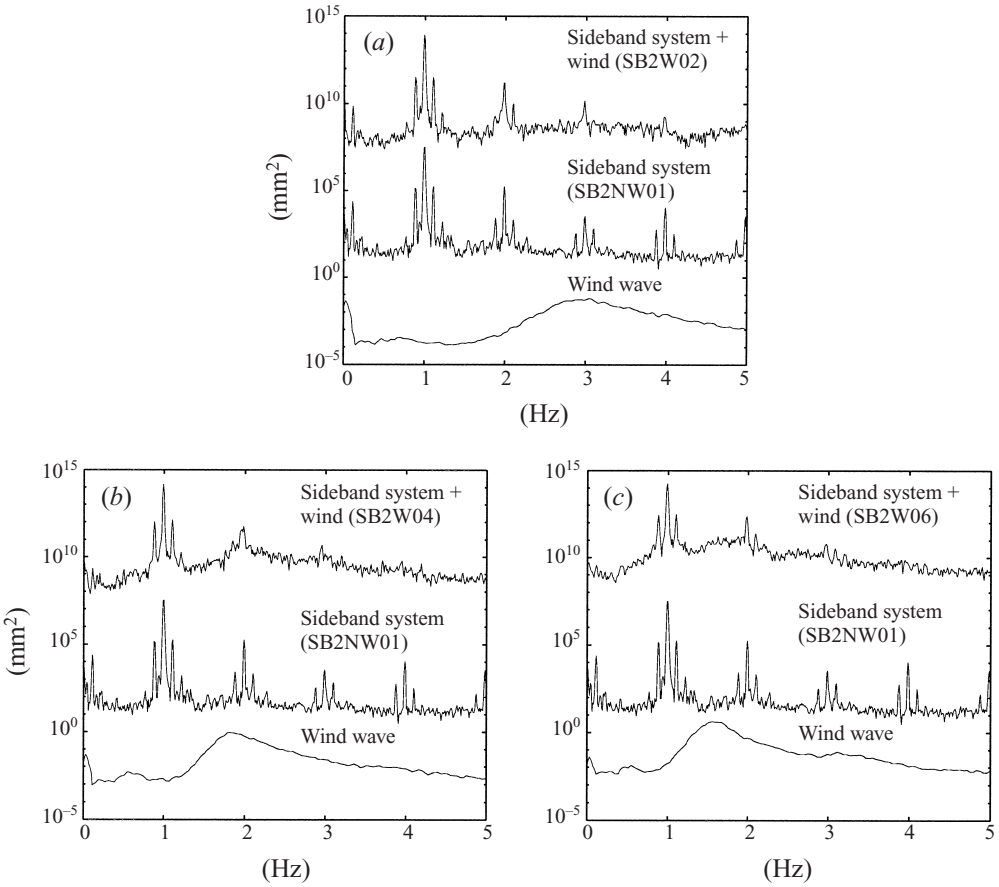

FIGURE 4. As figure 3 but for system (1.0 Hz, $\epsilon = 0.133$) with wind (SB2W02, SB2W04 and SB2W06), plotted together with the no-wind case (SB2NW01) and the wind-wave spectrum. Wind speeds are (*a*) 4.1, (*b*) 8.5, (*c*) 13.1 m s^{-1}. Fetch is 41.14 m.

bars denote the standard deviation of $\overline{b}$ obtained from five independent runs, and the straight line is the best fit exponential growth curve (3.5). The model equation was fitted to the data excluding that from the first wire (1.2 m fetch) since it was not located within the wind tunnel section. Therefore, the first fetch that appears in these figures is about 8 wavelengths away from the wave generator (12.64 m fetch), and the last fetch is about 26 wavelengths away (41.14 m fetch).

Figure 5 summarizes the evolution of the sidebands without wind (SB1NW). For all $\hat{\delta}$, the evolution is an exponential growth with some random variation of data from it, the variation quite large for the $\hat{\delta} = 1.029$ case. This exponential growth character is still maintained even when the wind is added to the sideband system; figure 6 shows the growth of SB1NW04 ($\epsilon = 0.175$ and $\hat{\delta} = 0.857$) with wind (SB1W). For all the cases, the initial sideband amplitude remains more or less unchanged as expected for the seeded runs. The same features, exponential growth and the large scatter of data points at higher wind speeds, are commonly observed in the smaller steepness cases, $\epsilon = 0.133$, and those are all summarized in figure 7 (SB2NW, SB2W).

The scatter of data points as indicated by an error bar comes from the real effects in the tank. For the no-wind case, the interval between successive measurements was

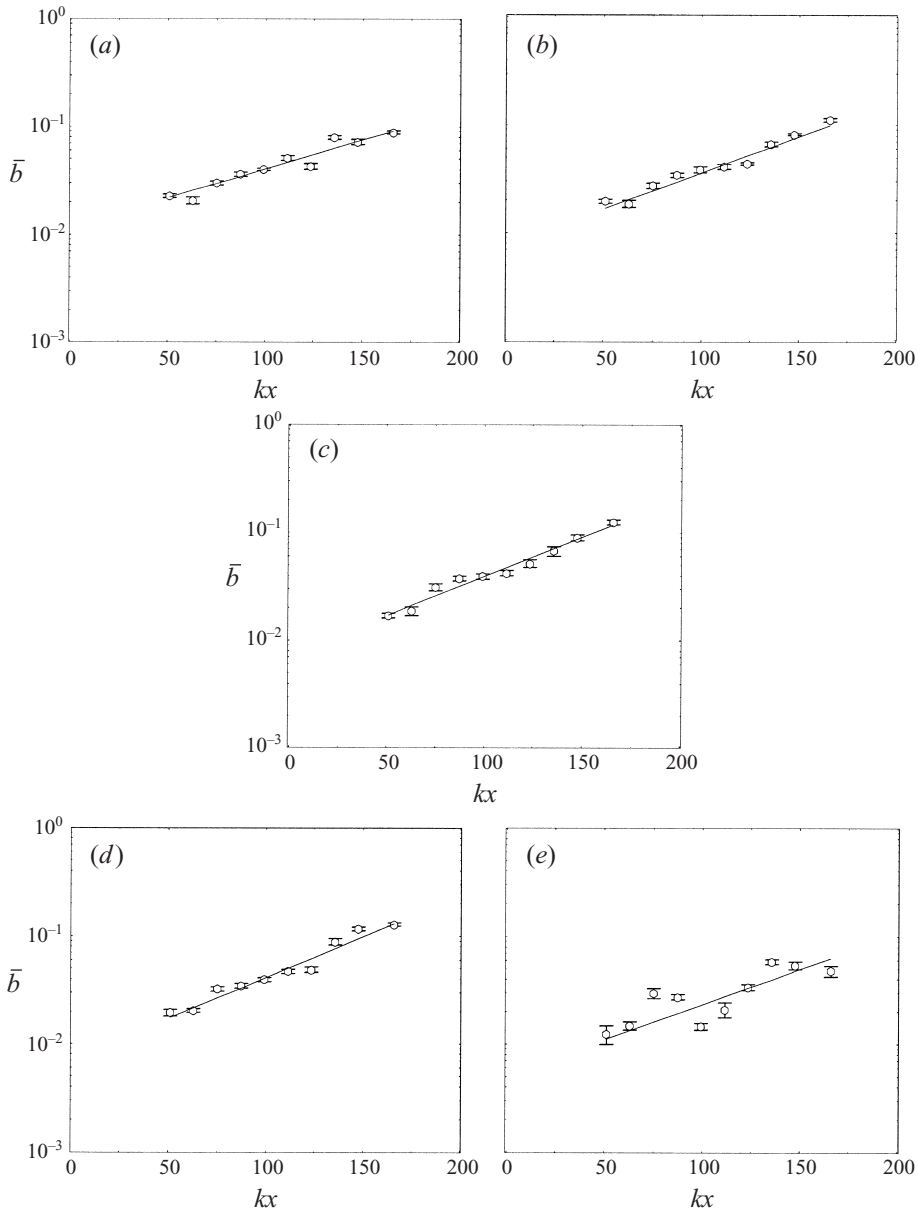

FIGURE 5. Growth of the mean normalized sideband amplitude versus non-dimensional fetch, for seeded sideband waves without wind (SB1NW). The error bar denotes the standard deviation from five independent runs. The straight line is an exponential growth fit. The waves were 1.0 Hz, $\epsilon = 0.175$, and $\hat{\delta} = 0.343, 0.514, 0.686, 0.857, 1.029$ (*a–e*).

about 10 minutes, and for the with-wind case, the interval between runs was 15 to 20 minutes. The interval is normally considered long enough for the residual wave energy to dissipate, since the reflected energy from the beach is typically less than 1%. Furthermore, no breaking was observed in any of the seeded runs. Therefore, it is not apparent why the previous run can affect the successive run, but as indicated by the

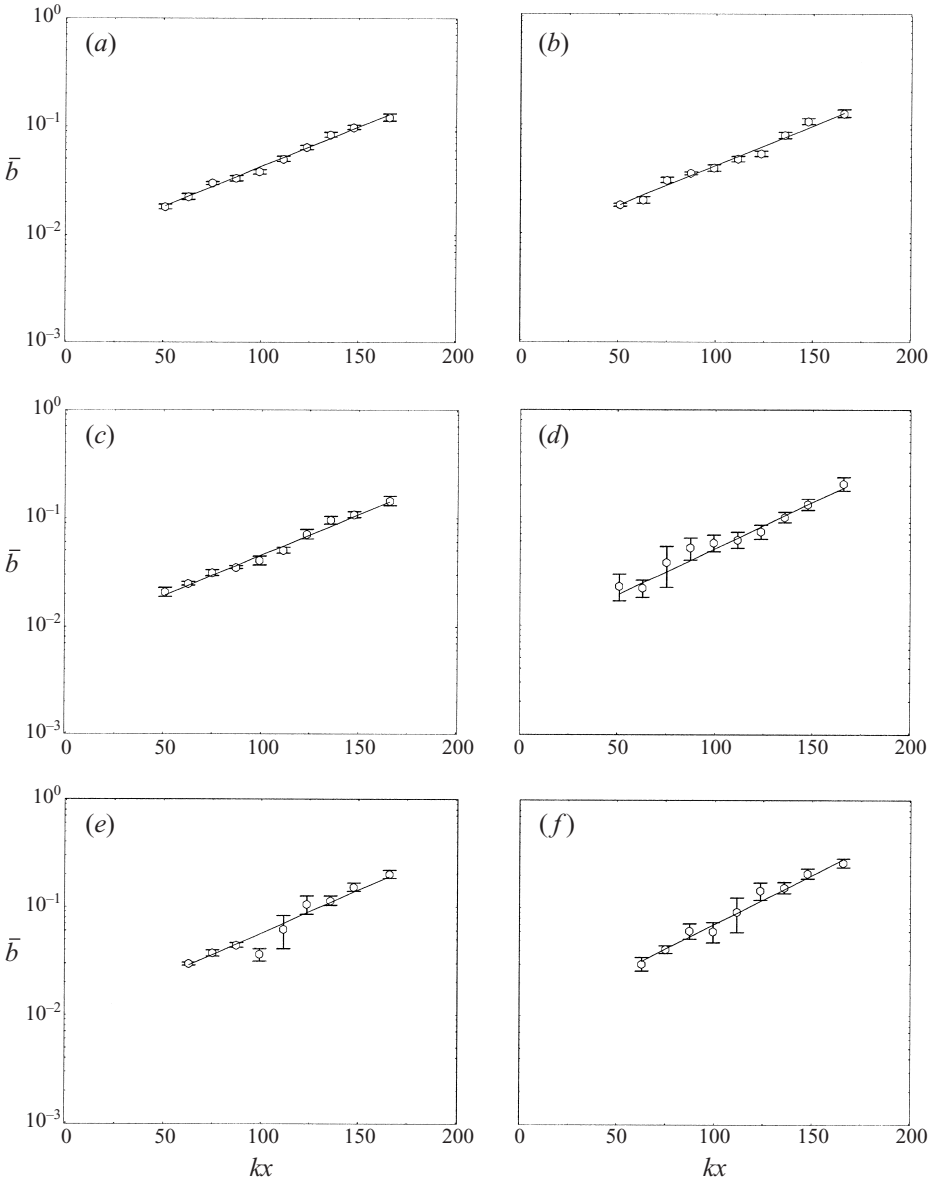

FIGURE 6. As figure 5 but for seeded sideband waves with wind (SB1W). The waves were 1.0 Hz, $\epsilon = 0.175$, $\hat{\delta} = 0.857$. The wind speeds were $U_{1m} = 1.8, 4.1, 6.3, 8.5, 10.8, 13.1\,\mathrm{m\,s^{-1}}$ (*a–f*), and the corresponding U_{1m}/C_p were 1.15, 2.63, 4.04, 5.45, 6.92, 8.40.

variability of each of five identical runs, these small residues in the tank from previous runs seem to influence the wave generation, and they should not be disregarded.

For the high wind speed cases, say higher than $10\,\mathrm{m\,s^{-1}}$, the effect of wind became large enough to distort the mechanically generated waves, such that sometimes the waves appeared to propagate at an angle. Particularly for the highest wind speed, there was an obvious signature of an asymmetry across the tank. These real effects will introduce a large scatter in the data, particularly for the large wind speeds, and the computed error bar for each data point is large (figures 6 and 7).

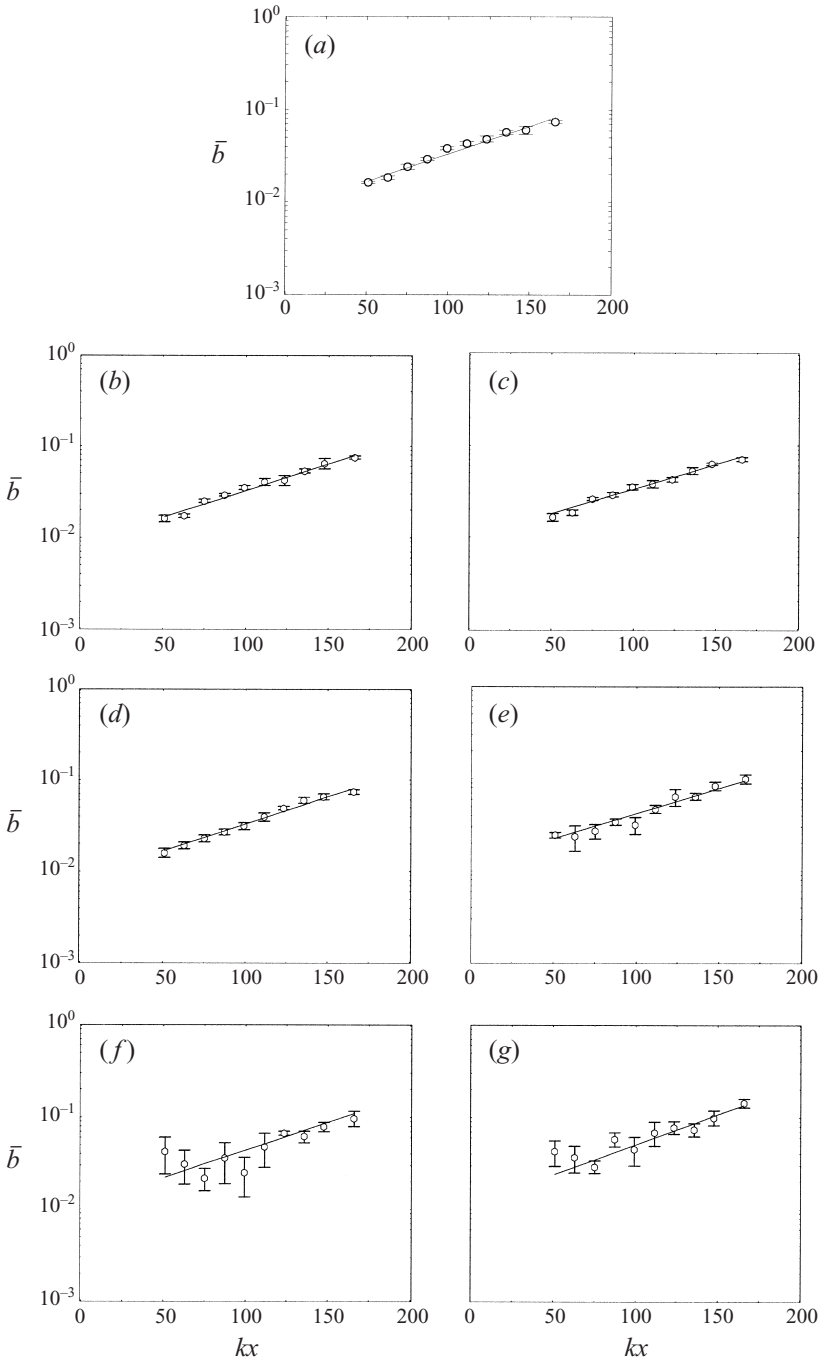

FIGURE 7. As figure 5 but for seeded sideband waves with and without wind (SB2NW, SB2W). The waves were 1.0 Hz $\epsilon = 0.133$, $\hat{\delta} = 0.842$. The wind speeds were $U_{1m} = 0$, 1.8, 4.1, 6.3, 8.5, 10.8, 13.1 m s^{-1} (*a*–*g*) and the corresponding U_{1m}/C_p were as figure 6.

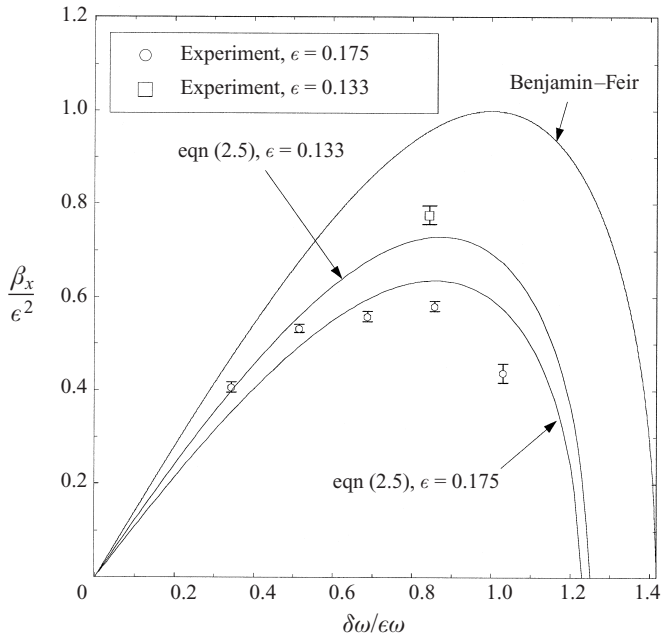

FIGURE 8. Growth rate of the sidebands without wind (seeded run). For waves 1.0 Hz, $\epsilon = 0.175$, $\hat{\delta} = 0.343, 0.514, 0.686, 0.857, 1.03$, and 1.0 Hz, $\epsilon = 0.133$, $\hat{\delta} = 0.842$. The curves are theoretical predictions from Benjamin & Feir (1967), and from (2.5) based on Krasitskii (1994).

4.2.3. *Growth rate*

Figure 8 summarizes the normalized growth rates β_x/ϵ^2 estimated from the fetch diagrams for the no-wind cases (SB1NW, SB2NW) plotted against $\hat{\delta}$. The error bar denotes the 68% confidence interval of the estimated growth rate. The solid lines are the theoretical prediction of the growth rate computed using theories by Benjami & Feir (1967) and (2.5). It is clear from this figure that Benjamin–Feir's theory overestimates the growth rate, but the Krasitskii (1994) theory (2.5) predicts the growth rate fairly well. There is a variety of theories that take into account the finite-amplitude effect, but few experimental data are available for validation. The current study, we believe, provides new data, spanning the parameter space for both ϵ and $\hat{\delta}$.

For $\epsilon = 0.175$, we can observe that the maximum growth rate is achieved for $\hat{\delta} = 0.857$, roughly corresponding to the maxima of the growth rate curve as predicted by (2.5). The $\epsilon = 0.133$, $\hat{\delta} = 0.842$ (SB2NW) case lies roughly at the maxima of the predicted growth curve. Those two cases that correspond to the maximum growth condition for each steepness were used to study the effect of wind. The obtained growth rates are summarized in figure 9. Here, the normalized estimated growth rates β_x/ϵ^2 are plotted versus normalized wind speeds U_{1m}/C_p or the inverse of the wave ages. For both $\epsilon = 0.175$ and 0.133, the growth rate showed a slight decrease and then an increase with increasing wind speed. The growth rate seems to have a minimum around moderate wind speeds (2–4 m s^{-1}); the initial reduction is only about 10%. The highest growth is obtained for both steepnesses at the maximum wind speed, but the estimation error becomes quite large. Neither case indicates strong reduction in

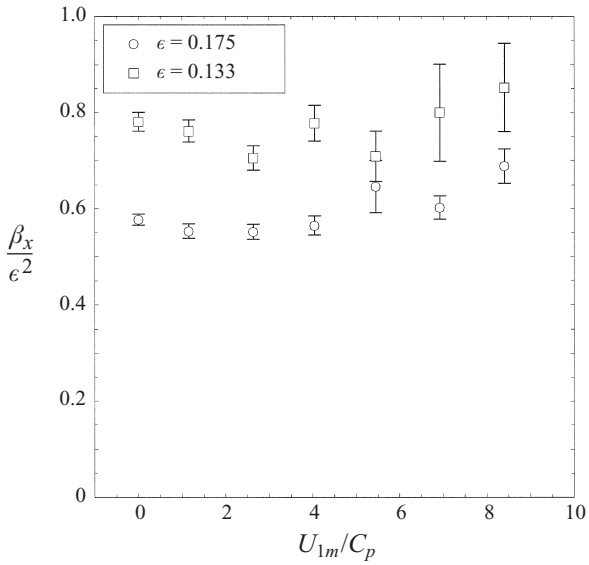

FIGURE 9. Growth rate of the sidebands with wind (seeded run). The waves were 1.0 Hz, $\epsilon = 0.175$, $\hat{\delta} = 0.857$, and 1.0 Hz, $\epsilon = 0.133$, $\hat{\delta} = 0.842$, for wind speeds $U_{1m} = 1.8, 4.1, 6.3, 8.5, 10.8, 13.1\,\mathrm{m\,s^{-1}}$.

the growth rate with wind as reported in the earlier works on unseeded experiments (Bliven *et al.* 1986; Li *et al.* 1988).

4.3. *Monochromatic wave with wind (unseeded run)*

4.3.1. $\epsilon = 0.20$, *type I instability*

The seeded runs as described in the previous section indicated that the effect of wind on the growth of the sidebands was not necessarily suppression. This turns out to be the case for the unseeded runs conducted in our tank as well, which we will describe below. First we will present the spectra of $\epsilon = 0.20$ waves at 41.14 m fetch for wind speeds 0, 1.8, 4.1, 6.3, 8.5, 10.8 and 13.1 $\mathrm{m\,s^{-1}}$ (figure 10). Except for the high wind speed runs, 10.8 and 13.1 $\mathrm{m\,s^{-1}}$ run, the naturally evolved sidebands are confined to a narrow energy band, somewhat similar to the seeded runs. The high-frequency peaks are also observed, and there is no significant filling of energy between these narrow peaks.

Unlike the seeded experiments, the spectrum was computed as an average of the data from about 50 minutes of a continuous run. As described earlier in the experimental procedure, the run was made for about 60 minutes and the first 10 minutes were excluded from the averaging. Tulin & Waseda (1999) described in detail that the natural selection of the sideband disturbance in a closed tank is associated with the multiple reflection of the wave front between the beach and the wave generator, and therefore the modulation becomes significant only after some delay. In our experiment, it typically took about 10 to 15 minutes or so till the modulation became visible at fetches, say, around 35 m or so. Since the perturbation propagates at the group velocity of the carrier wave back and forth between the beach and the wave generator, it is observed that the modulation cyclically strengthens and weakens as the wave front passes the observation point. The perturbation energy builds up with time, and occasionally the modulation becomes large enough at about 35 m fetch to cause breaking near the group peak. The breaking, however, is moderate and did

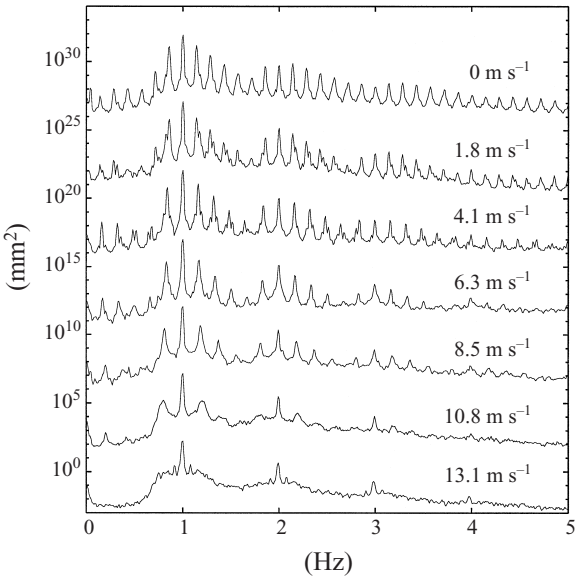

FIGURE 10. Specta of the monochromatic wave (1.0 Hz, $\epsilon = 0.20$) plus wind (M2W) at fetch 41.14 m; unseeded type I. The spectral estimates are 60 degrees of freedom, frequency resolution 0.01 Hz, and Hanning window was applied. The spectra have an offset of five decades. Wind speeds are 0.0, 1.8, 4.1, 6.3, 8.5, 10.8, 13.1 m s^{-1}.

not introduce any visible disturbance to the system. It was observed to occur earlier in the run when wind was added, but the breaker location was always at fetches 35–40 m or so, such that most of the surface elevation recording along the fetch was made prior to the breaker location.

As the wind speed increases, one can still observe a modulation, but the tendency is to diminish the modulation. This can be seen from the broadening of the sideband spectral peaks as the wind speed increases, and a complete disappearance of the sideband is observed at the highest wind speed, 13.1 m s^{-1}, see figure 10. At this highest wind speed, there was no visible modulation but still crest breaking was observed throughout the tank. There was more wind-wave-generated roughness on the waves, and these wind waves were the likely cause of the observed breaking. Such wind-wave breakers will introduce random perturbation to the system as can be seen from the energy filling in the gaps between spectral harmonics. These random perturbation may have caused the suppression of the sideband growth in the highest wind speed case, and therefore this extreme wind forcing case was excluded from the growth rate estimation since no sideband peaks were identified from the spectrum. For the rest, we were able to identify the sideband spectral peaks, and their frequencies ranged from $\hat{\delta} = 0.679$ to 0.965, well within the instability regime but over a large variation in wind speed, see table 1.

The broadening of the sideband peaks seems to come from the natural variability of the selected sideband perturbation in the unseeded case. As a result of the wind-induced disturbance in the tank, the sideband perturbation tends to vary randomly in time, causing the recorded sideband frequencies to fluctuate in time. When all the ensembles are averaged, this variability results in broadening of the sideband peaks. Therefore, it would appear from the averaged spectrum, figure 10, as if the sideband amplitudes decreased. But this does not necessarily imply the suppression of sideband

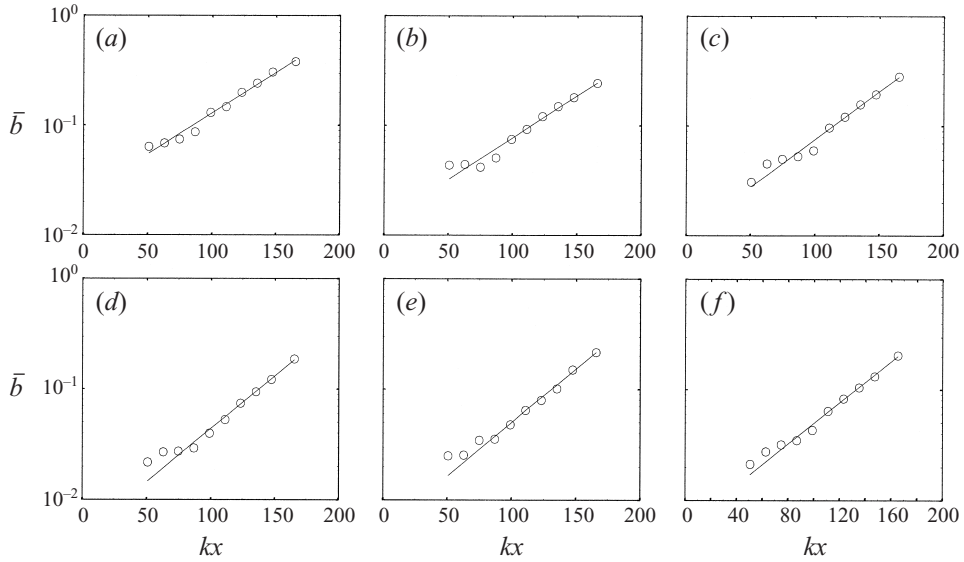

FIGURE 11. Growth of the mean normalized sideband amplitude versus non-dimensional fetch, for monochromatic waves (1.0 Hz, $\epsilon = 0.20$) with wind (M2W); unseeded type I. The straight line is an exponential growth fit. The wind speeds were $U_{1m} = 0$, 1.8, 4.1, 6.3, 8.5, 10.8 m s^{-1} (*a–f*), and the corresponding modulational frequencies were $\hat{\delta} = 0.6793$, 0.6793, 0.7626, 0.8102, 0.8938, 0.9652.

growth, as can be seen from figure 11. For all wind speeds, an exponential growth is still observed. Figure 11 also shows that the initial sideband amplitude tends to be smaller for higher wind speeds, and as a result, it appears that the growth rate is higher for higher wind speeds, quite contradictory to the previously reported unseeded results.

Figure 12 summarizes the growth rate estimated from the fetch diagram, plotted against non-dimensional wind speed. The growth rates are higher when wind is present, and the largest increase is about 30%, much higher than those observed in the seeded case, around 10% at most. One can also observe that the maximum growth is achieved not at the highest wind speed plotted, 10.5 m s^{-1}, but at a lower wind speed, 8.5 m s^{-1}. This observation is crucial for the understanding of the controversial results of our measurements when compared with the earlier observations by Bliven *et al.* (1986), and will be discussed in full later.

4.3.2. $\epsilon = 0.24$, *type II instability*

The wave spectra at 41.14 m fetch for the unseeded steepness $\epsilon = 0.24$ case are plotted in figure 13. Comparing the spectra for different wind speeds, the highest wind speed, 13.1 m s^{-1}, appears radically different and was not used for further comparisons. The modulational frequencies are around 0.27 to 0.29 Hz for 0, 4.1, and 8.5 m s^{-1} wind speeds and slightly increase with speed. The corresponding $\hat{\delta}$ is around 1.1 to 1.2, larger than the fastest growing condition as predicted by the theory (2.5), $\hat{\delta} < 1.0$.

From visual observation, the wave crest across the tank displayed a large amplitude variation. Breaking waves were observed at 35–40 m fetch, but unlike the breaking observed for the seeded $\epsilon = 0.20$ case that occurs at the crest of the wave group, the breaking occurs near the sidewall, where the breaker location alternated between opposite sides of the tank from crest to crest. The crest amplitude reduced from

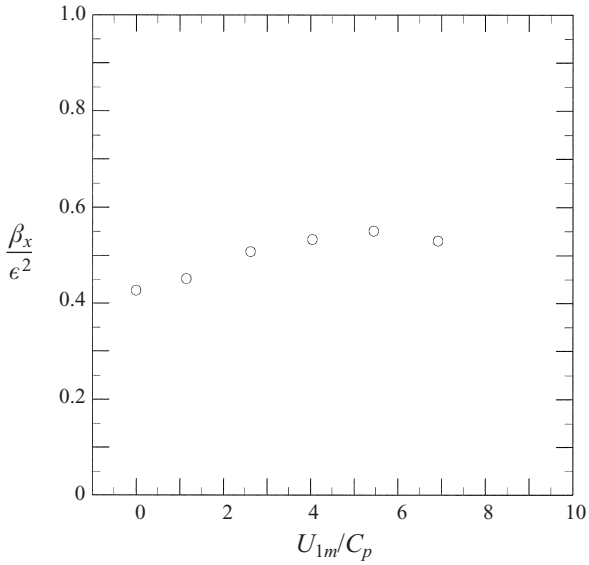

FIGURE 12. Growth rate of the sidebands of monochromatic waves (1.0 Hz, $\epsilon = 0.20$) with wind (M2W); unseeded type I. Wind speeds are $U_{1m} = 0$, 1.8, 4.1, 6.3, 8.5 and 10.8 m s^{-1}.

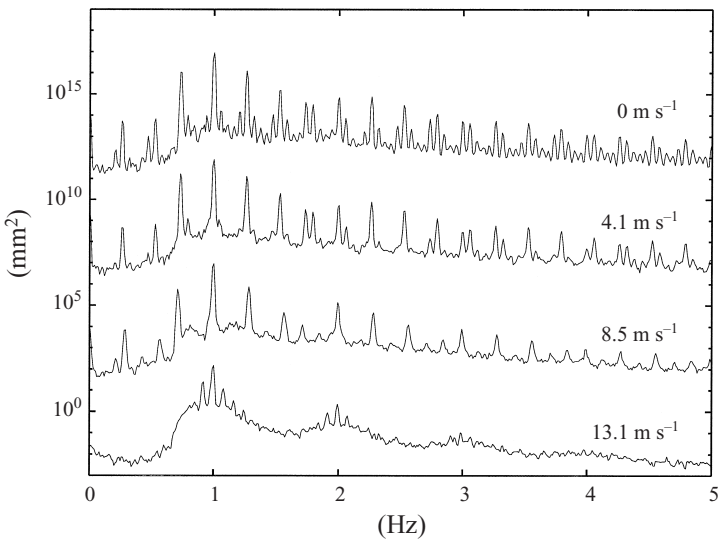

FIGURE 13. Spectrum of the monochromatic wave (1.0 Hz, $\epsilon = 0.24$) plus wind (M1W); unseeded type II. The spectral estimates are 60 degrees of freedom, frequency resolution 0.01 Hz, and Hanning window was applied. The spectrum has an offset of five decades. Wind speeds are 0, 4.1, 8.5, 13.1 m s^{-1}. Fetch 41.14 m.

one side of the tank to the other, and this pattern reversed in the next wave crest. This alternating crest amplitude pattern across the tank indicates the presence of an oblique wave perturbation or a three-dimensional instability.

The three-dimensional instability was studied extensively by Su (1982). He has shown that for $0.25 < \epsilon \leqslant 0.33$, a three-dimensional pattern was observed and the sideband waves that propagate at an angle had a wavenumber about 1.2 times the carrier wave. This corresponds to about 1.1 times the frequency of the carrier wave,

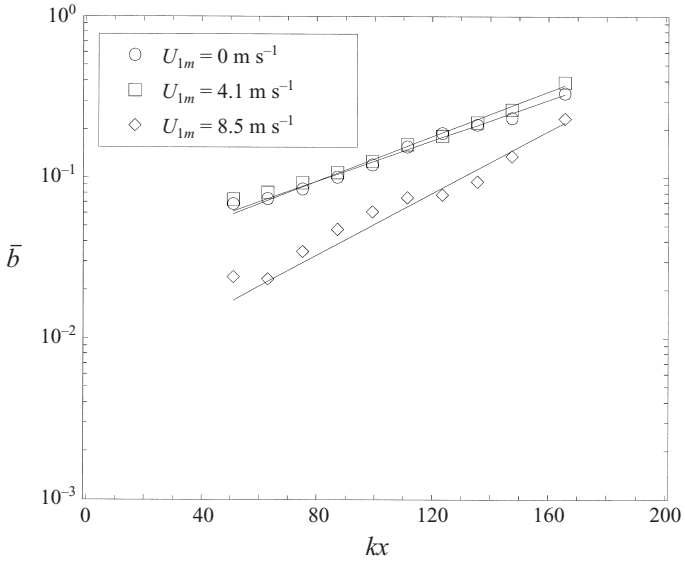

FIGURE 14. Growth of the mean normalized sideband amplitude versus non-dimensional fetch, for monochromatic waves (1.0 Hz, $\epsilon = 0.24$) with wind (M1W); unseeded type II. Wind speeds are 0, 4.1, 8.5 m s^{-1}.

which agrees quite well with our observation. This comparison indicates that the sideband wave modes seen in figure 13 are not of Benjamin–Feir (type I) but a type II instability. We observed in the same tank in a previous study that for unseeded high-steepness runs, a three-dimensional modulation occurred, and at highest steepness, say around $\epsilon = 0.30$, the crescent shape breaking as described by Su (1982) was observed. We have shown now that these three-dimensional instabilities will occur in the presence of wind.

The growth of the sidebands with fetch is summarized in figure 14. Similarly to the type I instability as described in the previous section, the initial sideband amplitude reduces with wind but the growth is enhanced. The growth is exponential, indicating that the cross-tank asymmetry observed in the tank was indeed due to the three-dimensional instability. Although this instability itself is of great interest, most of the energetic waves in the ocean are of much lower steepness, and we have therefore not pursued further study of these in the current work.

5. Discussion

5.1. *Unseeded experiments: comparison with previous studies*

The unseeded experiments showed an increase of growth rates for all wind speeds. The wind speed dependence was not monotonic, however, and above 8.5 m s^{-1}, the growth rate started to reduce, but was still larger than without wind, see figure 12.

This finding contrasts with that of Bliven *et al.* (1986) who conducted an unseeded experiment in a tank of length 20 m; their mechanically generated wave was around 40 cm in length, steepness around $\epsilon = 0.1$ to 0.24. There were four measuring stations and the largest fetch corresponded to about 35 wavelengths from the wave generator. The wind forcing was in the range $u_* = 16$ to 35 cm s^{-1} ($C_p/u_* = 2.23$ to 4.88, U_{1m} was not reported). In the current study, we have used waves 1.56 m long and steepness

around $\epsilon = 0.20$. The last measuring station was around 26 wavelengths from the wave generator. The wind forcing was $U_{1m} = 1.8$ to $13.1\,\mathrm{m\,s^{-1}}$ ($C_p/U_m = 0.12$ to 0.87, or $C_p/u_* = 2$ to 8). Our experiments cover a broader and weaker wind forcing range but the strongest wind forcing is about the same in both cases.

Although the use of short waves of less than 0.5 m is necessary in order to reproduce the previous experiment by Bliven *et al.* (1986), it was impossible because of experimental limitations (the wave maker is designed to have optimum performance generating waves between 60 cm and 10 wavelength). However, we believe that the scale of the previous experiment and that of this study are comparable, because the conflicting effect of wind-wave interactions and the intrinsic wave nonlinearity can be scaled by the wave age, as we discuss in § 5.2. As we show below, the apparently contradictory result of the two experiments can be explained by the same effect of the wind on the instability. This justifies our scaling argument.

Bliven *et al.* (1986) have shown that for $\epsilon = 0.24$, the growth rate nearly halved compared to the no-wind case when the strongest wind was applied. In contrast to that, in our experiment at $\epsilon = 0.2$ (figure 12) we found the growth rate larger than in the no-wind case. Bliven *et al.* (1986) have computed the growth rates for a limited number of cases, and those we will compare with our results. In most of the other experimental results reported by them, the growth rates were not estimated. However, they have reported a suppression of the sideband energy. In the current study, although we have measured the growth rate to be larger than in the no-wind case, we have also observed suppression of the initial sideband amplitudes in the presence of wind as illustrated in figure 11. This clearly indicates that the wind will reduce the naturally developed initial sideband energy but the growth rate is not necessarily suppressed. This observation suggests that further study of the natural selection process of the sideband in the tank is crucial for estimating what may happen in the ocean.

One important factor not mentioned in the paper of Bliven *et al.* (1986) is the effect of changes in modulational frequency on the growth rate. In figure 15, we compare the modulational frequency measured by Bliven *et al.* (1986) with ours, plotted against u_*/C_p. The data from case M2W are compared with data from Bliven *et al.* (1986) and also from Melville (1982). These measurements seem consistent, taking into account differences in ϵ, although Bliven *et al.*'s (1986) measurements with wind are considerably higher than ours. As we saw earlier in figure 8, the growth rate for a given ϵ depends strongly on the modulational frequency, especially when the modulational frequency is larger than the fastest growing modulational frequency; this is because of the cut-off bound in the instability predictions, (2.5). The change in the growth rate with respect to the modulational frequency is moderate up to the fastest growing modulational frequency, but beyond that the change becomes more rapid and the growth rates decline. In order to study these effects, we have plotted the sideband growth rate of our unseeded experimental result and the Bliven *et al.* (1986) case P03 ($0.22 \leqslant \epsilon \leqslant 0.25$) versus modulational frequency, figure 16. The growth rate in the Bliven *et al.* (1986) case was estimated from the growth curve presented in figure 6 of Hara & Mei (1991).

Surprisingly, the estimated growth rates are well predicted by the Krasitskii theoretical estimate of the initial growth rate. Qualitatively, both experimental results agree reasonably with the respective theoretical predictions; compare the agreement with the seeded case, figure 8. In particular, the diagram displays one of the major differences in the two experiments: ours had modulational frequencies below the fastest growing modulational frequency, whereas Bliven *et al.*'s (1986) were higher

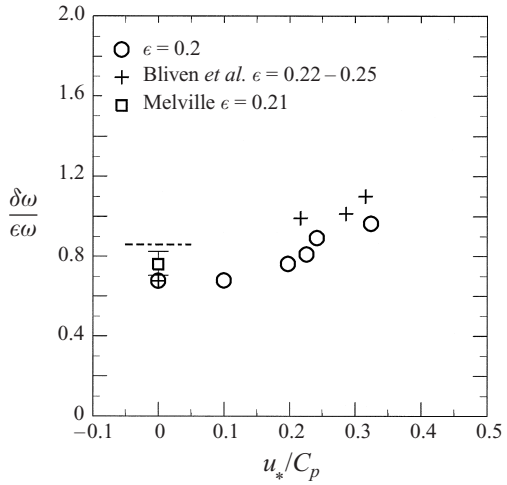

FIGURE 15. Modulational frequency plotted versus normalized friction velocity from the unseeded type I runs. Case M2W is compared with Bliven *et al.* (1986) and Melville (1982). Symbols are: ○, this study for $u_*/C_p = 0$, 0.100, 0.198, 0.226, 0.242, 0.324; +, Bliven *et al.* (1986) data for $u_*/C_p = 0$, 0.217, 0.286, 0.316; □, Melville (1982) for $u_*/C_p = 0$. The horizontal dashed line indicates the theoretically predicted maximum growth modulational frequency. The case $u_*/C_p = 0.100$ of this study corresponds to wind speed $1.8\,\mathrm{m\,s^{-1}}$ where u_*/C_p was inferred since the actual friction velocity was not measured.

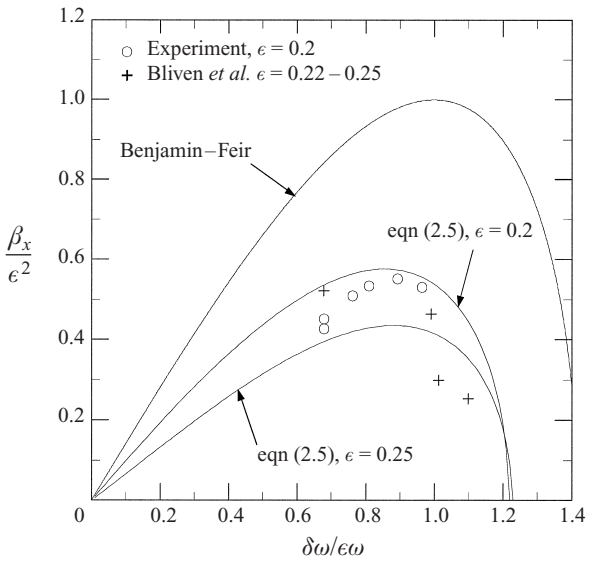

FIGURE 16. Growth rate of the sidebands of monochromatic waves (1.0 Hz, $\epsilon = 0.20$) with wind; unseeded type I. The curves are theoretical prediction by Benjamin–Feir and (2.5).

than or at the fastest growing modulational frequency. From this, we suggest that the reason for such a large suppression of sideband growth in the results of Bliven *et al.* (1986) is partially due to the deviation of the modulational frequency from the fastest growing condition.

Although Hara & Mei (1991) seem to have successfully reproduced the Bliven *et al.* (1986) experimental result (see figure 6 of Hara & Mei 1991) their estimation was made for a particular shape of the drift current profile (log-linear profile). The choice of the exact shape of the velocity profile in the water was crucial for their growth rate estimation, and when a linear profile was chosen, they saw an enhancement of the sideband growth. As pointed out by them, a precise knowledge of the induced turbulent current is essential to estimate the growth rate accurately. This leaves some question as to the significance of their agreement with the experimental observation. Furthermore, their theory is an extension of Dysthe's and the validity is limited to small steepness waves ($\epsilon < 0.1$) as mentioned by them and as also shown in figure 1 of this study. Finally, most important of all, Hara & Mei's choice of the modulational frequencies ($\delta\omega/\omega = 0.157{-}0.166$) was made for the maximum growth condition predicted by the theory and included viscous effects which predicted a narrower range than the experimental finding of Bliven *et al.* (1986) ($\delta\omega/\omega = 0.151{-}0.277$).

When changes of the modulational frequency are taken into account, the growth rate seems to change following the theoretical prediction as shown in figure 16, and both the unseeded experiment of Bliven *et al.* (1986) and ours are well described by an inviscid theory. This then suggests that the most important effect of wind is to alter the selection of naturally evolving modulational frequency. In figure 15 we compared the modulational frequency observed by Bliven *et al.* (1986) and ours. The wind speed dependence seems to suggest the existence of a law that determines the modulational frequency as a function of wave age. For young sea, i.e. large u_*/C_p, the modulational frequency $\hat{\delta}$ exceeds 1 and approaches larger values outside the instability region. But for moderate to old seas, say $u_*/C_p < 0.2$, the modulational frequency is not altered by the wind. This suggests that, in nature, where the wave is moderate to old, the sideband instability may not necessarily be suppressed by wind. The sideband growth rate may, of course, change as a result of proposed viscous effects as discussed by Hara & Mei (1991) and Li *et al.* (1988). However, such effects need experimental verification, and the growth rate we saw in the seeded experiment is within 10% of that in the no-wind case.

It is clear now that there are two wind effects on the modulation of the wave train. One alters the selection of the naturally evolving sideband frequency or the modulational frequency. The second modifies the inviscid growth by a viscous effect. The former seems to have a significant effect for young waves since the modulational frequency becomes large approaching the limit of the instability region, effectively reducing the growth rate considerably. The viscous effect becomes important for moderate to old waves and seems to have some wave-age dependence.

5.2. *Background perturbation and wave-age effect*

In order to understand the natural selection mechanism of the sidebands in the unseeded runs, profound knowledge of the background perturbation is needed. Below we summarize three possible sources of the background perturbations. First, the perturbation can grow following the wave-front propagation as discussed by Tulin & Waseda (1999). Such perturbation is necessary for the modulational instability to occur for the unseeded run in a fetch-limited tank, as observed and utilized in previous works (Melville 1982; Bliven *et al.* 1986). The perturbation, however, seems to have a systematic tendency as one can see from figure 15 where the no-wind cases of Melville, Bliven *et al.* and our result consistently had values of $\delta\omega/\epsilon\omega$ smaller than the theoretically predicted maximum growth perturbation denoted by a horizontal

dashed line. Also, there seems to be a tendency for the increase of $\delta\omega/\epsilon\omega$ with wind, yet to be studied. A second source of perturbation is the wind-wave spectrum. Such background wind waves may well serve as a seed for the sideband perturbation if their frequencies lie well within the instability region. However, in the current study, they were, even for the highest wind speed cases (13.1 m s^{-1}), outside the instability region, see figures 3 and 4, and the energy was suppressed in the presence of mechanically generated waves. A third source of perturbation is the breaking events. Although we have not studied in detail the frequency contents of such disturbances, they seem to serve well as a source of broad spectral background noise. In the current study, we have seen frequent breakers for the high steepness cases ($\epsilon = 0.2, 0.24$) with the highest wind speed (13.1 m s^{-1}). For those cases, the wind waves riding on top of the mechanically generated waves broke throughout the tank (M1W04, M2W07).

It seems, therefore, unlikely that all the unseeded experiments conducted had random background perturbation and only the cases M1W04 and M2W07 may have had random perturbation within the instability region. Can such random background perturbation prevent the growth of the sideband? Is there any wind speed dependence? The answer to these questions seems to depend on the initial magnitude and the frequency of the background perturbation as well as on how fast the perturbation can grow by wind compared to the rate of nonlinear energy transfer. The latter can be measured by comparing the magnitude of the corresponding growth rates. For simplicity, we assume that the growth due to the nonlinear effect follows the Benjamin–Feir prediction (2.3), and the growth due to wind input follows Snyder's law (2.10). Then, the ratio of the nonlinear effect to the wind input effect can be approximately described as

$$\Omega = \epsilon^2 / \left(10^{-3} \frac{U}{C_p} \right). \tag{5.1}$$

The values of Ω, for the seeded cases with wind, range between 2 and 27, and for the unseeded type I cases with wind, they range between 5 and 35, see table 1. Also, the value of Ω for the strongest wind speed case of Bliven *et al.* (1986) is around 5. Therefore, the coverage of the wind strength seems broad enough for both seeded and unseeded runs: $\Omega \sim O(1)$ to $O(10)$. The sideband growth was not suppressed in the seeded case despite large wind forcing at high wind speeds since the experiment was conducted with special care not to introduce unknown background perturbations. In the unseeded case, the broadening of the sideband peaks with increasing wind speed was observed, see figure 10. It may appear, then, that the broadening of sideband peaks is due to the enhanced growth of background perturbation by wind, but the lack of knowledge of the background perturbation prevents us from further conjecture. As discussed earlier, the characteristics of the background perturbations seem to depend on the wind speed as well, but precise knowledge of them is not the focus of the current experiment.

In order to study the effect of random perturbation on instability, inclusion of the wind effect seems relevant, and a good measure of their significance seems to be Ω or the wave age. The magnitude of Ω indicates how fast the non-interacting background waves can grow by wind forcing. When the growth of those waves is as fast as the sidebands, their amplitude will grow as large as the sidebands and the waves and the sidebands will start interacting with each other, leading to an unpredictable evolution of the wave modes, which may appear on average as a suppression of the sideband growth. However, these are speculations and require further investigations. We suggest

that in order to elucidate the effect of random perturbation on instability, a newly designed experiment is needed. Such experiments should include the control of the magnitude and the frequency of the random perturbation at the wave generator as well as the wind variation. These are subjects for future research.

6. Conclusion

The success of experiments on nonlinear water wave evolution lies in a profound knowledge of the facility and a good control of it. In the study of resonant free-surface wave interaction, the wave generator plays the most important role in determining the quality of the outcome of the experiment. Particularly for the experiment conducted here, where a precise knowledge of the initial wave spectrum is needed, it is crucial to control the exact motion of the wave generator.

With a carefully designed wave generator, we have successfully conducted seeded experiments on the instability of the Stokes wave where the initial perturbation was prescribed exactly by the control signal, both in frequency and in strength. With full control of the initial perturbations, we were able to experimentally estimate the growth rates of the perturbations through ranges of parameters, steepness and modulational frequency. These results compared well with the theoretical estimates of the growth rates as computed in this study based on the four-wave resonant interaction theory of Krasitskii. Therefore, the seeded experiments served well as the validation of the inviscid instability theory.

The Benjamin–Feir instability leads to the formation of wave groups but it was not considered to exist under wind forcing as concluded from the unseeded experiments of Bliven *et al.* (1986) and Li *et al.* (1988). Despite these experimental results, recent reports on low-grazing-angle radar imaging of wind waves suggest the existence of wind-driven wave groups (Werle 1995; Smith, Poulter & MaGregor 1996; Lamont-Smith, Fuchs & Tulin 1998). Motivated by these fine observational works, we have extended the pioneering experimental work of Bliven *et al.* (1986) and Li *et al.* (1988).

We therefore added wind to the seeded runs and also conducted unseeded runs for comparison with previous works. The results suggested two effects of wind: the first is the viscous effect found from the seeded runs and would account for $\pm 10\%$ change in the growth rate; the second is the alteration of the selected sideband frequencies found from the unseeded runs. For some cases the selected sideband perturbations were far from the maximum growth condition as predicted from the instability theory. The second effect may result in a large decrease in growth rate for some cases, and it may successfully explain the Bliven *et al.* (1986) result where they have observed nearly 50% reduction of the growth rate. We therefore conclude that the inviscid change in the sideband frequency is dominant over the viscous effect, particularly for younger waves. Further evolution processes of these wave groups involve the effect of breaking energy losses and are described in Tulin & Waseda (1999).

Findings that were not discussed in detail in this study should be addressed in future research. First, a type II instability was found for the unseeded high-steepness runs with and without wind. Second, strong suppression of wind-wave energy was found with a modulated wave train in the background. The second finding should be compared with the wind-wave and regular-wave interaction as well. It is of great interest for remote sensing in the ocean with microwave sensors and should also provide increased knowledge on roughness and its relation to the wind stress as well.

Finally, the effect of random perturbation on instability seems relevant for the ocean waves. The current study does not consider the control of the random perturbation but it should be addressed in a separate experiment including the wind effect.

We express our thanks to Dr Ofer Oshri for the valuable discussion on the theoretical derivation of the initial growth rate. We also express our thanks to Mr Dominic Regas and Mr Jörn Fuchs for their assistance in conducting the experiment. Dr M. Donelan encouraged us at the early stage of the work. This work was supported partially by the Ocean Technology Program of the Office of Naval Research, Thomas Swean, program manager; and Advanced Sensor Applications Program Support, Donna Kulla, program manager. A part of the document preparation was done with support of the Frontier Research System for Global Change, which also partly sponsors the International Pacific Research Center. This manuscript is SOEST contribution No. 4830 and IPRC contribution No. 13.

Appendix. Derivation of the initial growth rate

The Krasitskii (1994) four-wave reduced equation reads

$$\mathrm{i}\frac{\partial b_0}{\partial t} = \omega_0 b_0 + \int \tilde{V}^{(2)}_{0,1,2,3} b_1^* b_2 b_3 \delta_{0+1-2-3}\,\mathrm{d}k_{123}. \tag{A 1}$$

The full expressions for the complex variable b_i and the interaction coefficient $\tilde{V}_{0,1,2,3}$ are presented in Krasitskii (1994) and will be omitted here. To the lowest order in amplitude, the complex variable b_i can be expressed in terms of the Fourier component of the free surface as

$$b_i = \frac{1}{2}\left(\frac{2\omega_i}{k_i}\right)^{1/2} a\mathrm{e}^{\mathrm{i}\alpha}\mathrm{e}^{-\mathrm{i}\omega_i t}, \tag{A 2}$$

where $\omega_i^2(\boldsymbol{k}) = g|\boldsymbol{k}|$, $a(\boldsymbol{k})$ is the real amplitude, and α is the phase. For a discrete three-wave system, (A 1) reduces to the following set of equations:

$$\left.\begin{aligned}
&\frac{\partial a}{\partial t} = 0, \quad \frac{\partial \alpha}{\partial t} = -\frac{\omega_0}{2k_0}k_0^3 a^2 T_{1111},\\
&\frac{\partial b_+}{\partial t} = k_0^3 a^2 b_- \frac{\omega_0}{2k_0}\left(\frac{\omega_-}{2k_-}\right)^{1/2}\left(\frac{\omega_+}{2k_+}\right)^{-1/2} T_{1123}\sin\phi,\\
&\frac{\partial \beta_+}{\partial t} = -2\frac{\omega_0}{2k_0}k_0^3 a^2 T_{1212} - \frac{\omega_0}{2k_0}\left(\frac{\omega_-}{2k_-}\right)^{1/2}\left(\frac{\omega_+}{2k_+}\right)^{-1/2} k_0^3 a^2 \frac{b_-}{b_+} T_{1123}\cos\phi,\\
&\frac{\partial b_-}{\partial t} = k_0^3 a^2 b_+ \frac{\omega_0}{2k_0}\left(\frac{\omega_+}{2k_+}\right)^{1/2}\left(\frac{\omega_-}{2k_-}\right)^{-1/2} T_{1123}\sin\phi,\\
&\frac{\partial \beta_-}{\partial t} = -2\frac{\omega_0}{2k_0}k_0^3 a^2 T_{1313} - \frac{\omega_0}{2k_0}\left(\frac{\omega_+}{2k_+}\right)^{1/2}\left(\frac{\omega_-}{2k_-}\right)^{-1/2} k_0^3 a^2 \frac{b_+}{b_-} T_{1123}\cos\phi,
\end{aligned}\right\} \tag{A 3}$$

where a, b_+, and b_- are the amplitudes of the carrier, the upper, and the lower sidebands; α, β_+, and β_- are the phases of the carrier, the upper, and the lower sidebands; $\phi \equiv 2\alpha - \beta_+ - \beta_- - \Delta\omega t$; T_{ijkl} is the normalized interaction coefficient defined as $\tilde{V}^{(2)}_{ijkl} \equiv k_0^3 T_{ijkl}$.

Equation (A 3) is an evolution in time rather than in space. In order to obtain an evolution equation in space, we assume that the propagation speed of each mode is

the linear group velocity, $\omega_0/2k_0$, $\omega_+/2k_+$, $\omega_-/2k_-$. We get

$$\left.\begin{aligned}
\frac{\partial a}{\partial x} &= 0, \quad \frac{\partial \alpha}{\partial x} = -k_0^3 a^2 T_{1111},\\
\frac{\partial b_+}{\partial x} &= k_0^3 a^2 b_- \frac{\omega_0}{2k_0}\left(\frac{\omega_-}{2k_-}\right)^{1/2}\left(\frac{\omega_+}{2k_+}\right)^{-3/2} T_{1123}\sin\phi,\\
\frac{\partial \beta_+}{\partial x} &= -2\frac{\omega_0}{2k_0}\left(\frac{\omega_+}{2k_+}\right)^{-1} k_0^3 a^2 T_{1212} - \frac{\omega_0}{2k_0}\left(\frac{\omega_-}{2k_-}\right)^{1/2}\left(\frac{\omega_+}{2k_+}\right)^{-3/2} k_0^3 a^2 \frac{b_-}{b_+} T_{1123}\cos\phi,\\
\frac{\partial b_-}{\partial x} &= k_0^3 a^2 b_+ \frac{\omega_0}{2k_0}\left(\frac{\omega_+}{2k_+}\right)^{1/2}\left(\frac{\omega_-}{2k_-}\right)^{-3/2} T_{1123}\sin\phi,\\
\frac{\partial \beta_-}{\partial x} &= -2\frac{\omega_0}{2k_0}\left(\frac{\omega_-}{2k_-}\right)^{-1} k_0^3 a^2 T_{1313} - \frac{\omega_0}{2k_0}\left(\frac{\omega_+}{2k_+}\right)^{1/2}\left(\frac{\omega_-}{2k_-}\right)^{-3/2} k_0^3 a^2 \frac{b_+}{b_-} T_{1123}\cos\phi,
\end{aligned}\right\} \tag{A 4}$$

where terms higher than $O(ak^2)$ were dropped. The phase terms should be combined as

$$\begin{aligned}
\frac{\partial \phi}{\partial x} = 2k_0^3 a^2 &\left(- T_{1111} + \frac{\omega_0}{2k_0}\left(\frac{\omega_+}{2k_+}\right)^{-1} T_{1212} + \frac{\omega_0}{2k_0}\left(\frac{\omega_-}{2k_-}\right)^{-1} T_{1313}\right) + k_0^3 a^2 \frac{\omega_0}{2k_0}\\
&\times\left(\frac{b_-}{b_+}\left(\frac{\omega_-}{2k_-}\right)^{1/2}\left(\frac{\omega_+}{2k_+}\right)^{-3/2} + \frac{b_+}{b_-}\left(\frac{\omega_+}{2k_+}\right)^{1/2}\left(\frac{\omega_-}{2k_-}\right)^{-3/2}\right) T_{1123}\cos\phi - \frac{\Delta k}{k}.
\end{aligned} \tag{A 5}$$

The solutions for (A 4) and (A 5) are

$$\left.\begin{aligned}
b_+ &= b_+(0)\cosh\left[\epsilon^2 (C_+C_-)^{1/2}\int_0^{\tilde{x}} \sin\phi\,\mathrm{d}\tilde{x}\right]\\
&\quad + \left(\frac{C_+}{C_-}\right)^{1/2} b_-(0)\sinh\left[\epsilon^2 (C_+C_-)^{1/2}\int_0^{\tilde{x}} \sin\phi\,\mathrm{d}\tilde{x}\right],\\
b_- &= b_-(0)\cosh\left[\epsilon^2 (C_+C_-)^{1/2}\int_0^{\tilde{x}} \sin\phi\,\mathrm{d}\tilde{x}\right]\\
&\quad + \left(\frac{C_-}{C_+}\right)^{1/2} b_+(0)\sinh\left[\epsilon^2 (C_+C_-)^{1/2}\int_0^{\tilde{x}} \sin\phi\,d\tilde{x}\right],
\end{aligned}\right\} \tag{A 6}$$

where $\epsilon \equiv k_0 a$, $\tilde{x} \equiv k_0 x$, $C_+ \equiv (\omega_0/2k_0)(\omega_-/2k_-)^{1/2}(\omega_+/2k_+)^{-3/2}T_{1123}$ and $C_- \equiv (\omega_0/2k_0)(\omega_+/2k_+)^{1/2}(\omega_-/2k_-)^{-3/2}T_{1123}$. For an instability to occur, the integral of $\sin\phi$ should be unbounded. The condition is satisfied when $\mathrm{d}\phi/\mathrm{d}x = 0$, which gives

$$\left.\begin{aligned}
b_+ &= (C_+/C_-)^{1/2}\, b_- = b_+(0)\exp[\beta_K \tilde{x}] = (C_+/C_-)^{1/2} b_-(0)\exp[\beta_K \tilde{x}],\\
\cos\phi &= 0.5\left[\frac{\Delta k/k}{\epsilon^2} - \left(\frac{\omega_0}{2k_0}\left(\frac{\omega_+}{k_+}\right)^{-1} T_{1212} + \frac{\omega_0}{2k_0}\left(\frac{\omega_-}{k_-}\right)^{-1} T_{1313} - 2\,T_{1111}\right)\right](C_+C_-)^{-1/2},\\
\beta_K &= \epsilon^2 (C_+C_-)^{1/2}\sin\phi.
\end{aligned}\right\} \tag{A 7}$$

REFERENCES

Benjamin, T. B. 1967 Instability of periodic wavetrains in nonlinear dispersive systems. *Proc. R. Soc. Lond.* A **299**, 59–75.

Benjamin, T. B. & Feir, J. E. 1967 The disintegration of wave trains on deep water. Part 1. Theory. *J. Fluid Mech.* **27**, 417–430.

Benney, D. J. 1962 Nonlinear gravity wave interactions. *J. Fluid Mech.* **14**, 577–584.

Bliven, L. F., Huang, N. E. & Long, S. R. 1986 Experimental study of the influence of wind on Benjamin–Feir sideband instability. *J. Fluid Mech.* **162**, 237–260.

Dysthe, K. B. 1979 Note on a modification to the nonlinear Schrödinger equation for application to deep water waves. *Proc. R. Soc. Lond.* A **369**, 105–114.

Hammack, J. L. & Henderson, D. M. 1993 Resonant interactions among surface water waves. *Ann. Rev. Fluid Mech.* **25**, 55–97.

Hara, T. & Mei, C. C. 1991 Frequency downshift in a narrowbanded surface wave under the influence of wind. *J. Fluid Mech.* **230**, 429–477.

Janssen, P. A. E. M. 1983 On a fourth-order envelope equation for a deep-water waves. *J. Fluid Mech.* **126**, 1–11.

Krasitskii, V. P. 1994 On reduced equations in the Hamiltonian theory of weakly nonlinear surface waves. *J. Fluid Mech.* **272**, 1–20.

Lake, B. M. & Yuen, H. C. 1977 A note on some nonlinear water-wave experiments and the comparison of data with theory. *J. Fluid Mech.* **83**, 75–81.

Lake, B. M., Yuen, H. C., Rungaldier, H. & Ferguson, W. E. 1977 Nonlinear deep-water waves: theory and experiment. Part 2. Evolution of a continuous wave train. *J. Fluid Mech.* **83**, 49–74.

Lamont-Smith, T., Fuchs, J. & Tulin, M. P. 1998 Laboratory investigation of lga scattering from wind-generated waves and wave groups. In *IGARSS '98*, vol. I, pp. 1219–1221.

Li, J. C., Hui, W. H. & Donelan, M. A. 1988 Effects of velocity shear on the stability of surface deep water wave trains. In *Nonlinear Water Waves* (ed. K. Horikawa & H. Maruo), pp. 213–220. Springer.

Longuet-Higgins, M. S. 1980 Modulation of the amplitude of steep wind waves. *J. Fluid Mech.* **99**, 705–713.

McLean, J. W. 1982 Instabilies of finite-amplitude water wave. *J. Fluid Mech.* **114**, 315–330.

Melville, W. K. 1982 The instability and breaking of deep-water waves. *J. Fluid Mech.* **115**, 165–185.

Oshri, O. 1996 Frequency downshifting in surface waves and free surface flows without waves. PhD thesis, University of California, Santa Barbara.

Phillips, O. M. 1967 Theoretical and experimental studies of gravity wave interactions. *Proc. R. Soc. Lond.* A **299**, 104–119.

Phillips, O. M. & Banner, M. L. 1974 Wave breaking in the presence of wind drift and swell. *J. Fluid Mech.* **66**, 625–640.

Smith, M. J., Poulter, E. M. & McGregor, J. A. 1996 Doppler radar measurements of wave groups and breaking waves. *J. Geophys. Res.* **101** (C6), 14269–14282.

Snyder, R. L., Dobson, F. W., Elliott, J. A. & Long, R. B. 1981 Array measurement of atmospheric pressure fluctuations above surface gravity waves. *J. Fluid Mech.* **102**, 1–59.

Su, M.-Y. 1982 Three-dimensional deep-water waves. Part 1. Experimental measurement of skew and symmetric wave patterns. *J. Fluid Mech.* **124**, 73–108.

Su, M.-Y., Bergin, M., Marler, P. & Myrick, R. 1982 Experiments on nonlinear instabilities and evolution of steep gravity-wave trains. *J. Fluid Mech.* **124**, 45–72.

Su, M.-Y. & Green, A. W. 1984 Coupled two- and three-dimensional instabilities of surface gravity waves. *Phys. Fluids* **27**, 2595–2597.

Toba, Y., Hatori, M., Imai, Y. & Tokuda, M. 1986 Experimental study of elementary processes in wind-wave using wind over regular waves. In *Wave Dynamics and Radio Probing of the Ocean Surface* (ed. O. M. Phillips & K. Hasselmann), chap. 6, p. 117. Plenum.

Tulin, M. P. & Waseda, T. 1999 Laboratory observations of wave group evolution, including breaking effects. *J. Fluid Mech.* **378**, 197–232.

Werle, B. 1995 Sea backscatter, spikes and wave group observations at low grazing angles. In *IEEE Intl Radar Conference*, pp. 187–195.

Yuen, H. C. & Lake, B. M. 1982 Nonlinear dynamics of deep-water gravity waves. *Adv. Appl. Mech.* **22**, 67–229.

Zakharov, V. E. 1968 Stability of periodic waves of finite amplitude on the surface of deep fluid. *J. Appl. Mech. Tech. Phys.* **2**, 190–194.